RESSALVA

Atendendo solicitação do
autor, o texto completo
desta dissertação será
disponibilizado somente a
partir de 31/03/2028.

UNIVERSIDADE ESTADUAL PAULISTA – UNESP

Instituto de Biociências, Letras e Ciências Exatas -

Campus de São José do Rio Preto

CAIQUE MOUREIRA TAVARES

MULTIFUNCTIONAL LUMINESCENT INKS BASED ON DOWNSHIFTING AND UPCONVERSION PROCESSES APPLICABLE IN ANTI-COUNTERFEITING PRINTING TECHNOLOGY

Presidente Prudente

2026

CAIQUE MOUREIRA TAVARES

MULTIFUNCTIONAL LUMINESCENT INKS BASED ON DOWNSHIFTING AND UPCONVERSION PROCESSES APPLICABLE IN ANTI-COUNTERFEITING PRINTING TECHNOLOGY

Dissertação apresentada à Universidade Estadual Paulista (UNESP), Instituto de Biociências, Letras e Ciências Exatas, São José do Rio Preto, para obtenção do título de Mestre em Química.

Área de Concentração: Química

Orientadora: Profa. Dra. Ana Maria Pires

Coorientador: Prof. Dr. Sergio Antonio Marques de Lima

Presidente Prudente

2026

T231m

Tavares, Caique
Multifunctional luminescent inks based on downshifting and upconversion processes applicable in anti-counterfeiting printing technology / Caique Tavares. -- São José do Rio Preto, 2026
150 f. : il., tabs., fotos

Dissertação (mestrado) - Universidade Estadual Paulista (UNESP), Instituto de Biociências Letras e Ciências Exatas, São José do Rio Preto
Orientadora: Ana Maria Pires
Coorientador: Sergio Lima

1. Íons terras raras. 2. Plataformas multifuncionais. 3. Combustão da ureia. I. Título.

Sistema de geração automática de fichas catalográficas da Unesp. Dados fornecidos pelo autor(a).

IMPACTO POTENCIAL DESTA PESQUISA

A falsificação tem se tornado uma crescente problemática nas áreas econômica, da saúde, ambiental e artística. Desse modo, tecnologias de impressão baseadas em íons lantanídeos, na forma de tintas luminescentes, têm se mostrado uma estratégia promissora em sistemas de segurança (*anti-counterfeiting*) devido às suas propriedades estruturais, espectroscópicas e fotofísicas favoráveis, além de apresentarem viabilidade econômica, baixo impacto ambiental e exequibilidade acessível.

POTENTIAL IMPACT OF THIS RESEARCH

Counterfeiting has become a growing problem in the economic, health, environmental, and artistic fields. Therefore, printing technologies based on lanthanide ions, in the form of luminescent inks, have emerged as a promising strategy in security systems (anti-counterfeiting), due to their favorable structural, spectroscopic, and photophysical properties, in addition to their economic viability, low environmental impact, and practical feasibility.

CAIQUE MOUREIRA TAVARES

MULTIFUNCTIONAL LUMINESCENT INKS BASED ON DOWNSHIFTING AND UPCONVERSION PROCESSES APPLICABLE IN ANTI-COUNTERFEITING PRINTING TECHNOLOGY

Dissertação apresentada à Universidade Estadual Paulista (UNESP), Instituto de Biociências, Letras e Ciências Exatas, São José do Rio Preto, para obtenção do título de Mestre em Química.

Área de Concentração: Química

Data da defesa: 31/03/2026

Banca Examinadora:

_____

Profa. Dra. Ana Maria Pires
UNESP – Faculdade de Ciências e Tecnologia – Campus de Presidente Prudente

_____

Profa. Dra. Caroline Silva Danna
UACh – *Facultad de Ciencias de la Ingeniería* – Valdívia

_____

Prof. Dr. Danilo Manzani
IQSC-USP – São Carlos

To my parents, Francineide and Antonio, who live my dreams every day.

ACKNOWLEDGMENTS

My family, especially my parents Francineide and Antonio, for unconditionally supporting my choices and being a support during difficult times over these years. To my friends, whether from my city or from the university, for celebrating my achievements with me or simply listening to me when things weren't going well. I highlight the "*Café da Tarde*" group: Gustavo, Maria, and Lívia, for being with me since my first year of undergraduate. *Thank you for everything and for your friendship!*

To Professor Ana Maria, for guiding me as a professional and, above all, as a person, since my undergraduate scholarship. What you did for me at the beginning of my master's degree is something I will never forget because, if I reached the end of this master's program, it was because I had your support. Every time I listen to Bon Jovi, I'll remember you and your rides to internship. To Professor Sergio, for co-supervising me and for being the most patient person I know, in addition to having an enviable brain, where he readily answered my questions (*however confusing they were*).

To Professor Camilo, for helping me with everything during my exchange program in Santiago, for going to great lengths to make me feel at home, and for teaching me to have a "spectroscopic eye" (*even if it sometimes fails*). To Professor Igor and Professor Caroline, for being like family during my stay in Valdivia and for giving me opportunities to work and collaborate. *Muchas gracias, Profes, un gustazo!*

To my beloved Laboratory of Luminescence in Materials and Sensors (LLuMeS): Augusto (Gutão), Alessandra (Alê/Milennial), Airton, André (Vô), Ariane (Ivete Sangalo), Maria Eduarda (Duda), Felipe, Leonardo (Bones), Renan, Vytor (Vaitor), Eduardo, Edy (Edão), Gustavo (Amigão), Júlia (Jú), Maísa (Maísão), Matheus (Pitoco), Guilherme (Targa), Thiago (Bigodinho), Rafaela and Gabriel. Thank you for all the coffees, "*conosquinhos*", scientific discussions and for helping me with absolutely everything. *I love you all very much!*

To the Professors on the qualifying exam: Professor Italo Odone and Professor Danilo Manzani. To the Professors on the defense exam: Professor Caroline and again to Professor Danilo. Thank you for the discussions and contributions to my work and professional development.

To teacher Tiago Costilhas, my English teacher, who guided me through most of my master's degree. Thank you for your patience, support during my exchange program,

words of encouragement, and for showing me that language is there to help, to open opportunities for new things, never the opposite. *Thanks a bunch, mate*!

To the guys from Apartment 104, especially Gabriel (Gab), who has been with me since my very first day living in Prudente. We've shared achievements, (many) complaints, and even a few unpaid tabs together.

To PhD students Douglas Henrique Sales (LCGRS) and Gisele Santos Silveira (LaCCeF) for the X-ray diffraction measurements. To PhD student Naralyne Martins Pesqueira (LACOM) and master's student Lívia Gonzalez Brunetti (LACOM) for the IR absorption measurements. To postdoctoral researcher Felipe da Silva Manrique Canisares (Leb-f) for the transmission electron microscopy images. To master's student Bruna Oliveira Salla do Carmo (NOIX) for the zeta potential measurements of the luminescent inks. To Professor Marco Utrera (UFMS) for enabling the zeta potential measurements by varying the pH and DLS. To PhD student Nagyla Alves de Oliveira (LMF) and postdoctoral researcher Sergio Fernando Nunes Coelho (LMF) for photoluminescence measurements. To PhD Douglas Henrique Vieira (LaDSor) for collaborating with the screen printing and spray coating techniques.

The grammatical revision of this dissertation was supported by ChatGPT-4, with all conceptual content reviewed and validated by the author and advisor. This work was carried out with the support of the Coordenação de Aperfeiçoamento de Pessoal de Nível Superior – Brazil (CAPES) – Funding Code 001.

RESUMO

A falsificação é considerada um problema relevante que impacta diretamente a economia em escala global, uma vez que moedas, cheques, cédulas, obras de arte e documentos podem apresentar vulnerabilidades, exigindo autenticação especializada. Nesse contexto, materiais luminescentes são considerados ideais para essa aplicação, pois podem apresentar emissão multicolorida, tempo de resposta rápido e sensibilidade a diferentes estímulos externos. Dessa forma, o objetivo deste trabalho foi desenvolver tintas luminescentes com emissão dual a partir de luminóforos do tipo $GdAlO_3$ contendo íons Eu^{3+} (*downshifting*, DS) ou Er^{3+}/Yb^{3+} (*upconversion*, UC), modificados ou não com SiO_2, para aplicação em sistemas de impressão voltados à antifalsificação (*anti-counterfeiting*). Utilizou-se o método de combustão da ureia, autossustentado e ambientalmente favorável, para síntese dos luminóforos, bem como o método Stöber para modificação da superfície com SiO_2. As tintas luminescentes foram formuladas a partir de duas matrizes poliméricas: álcool polivinilico (PVA) e glicerol. As técnicas de impressão avaliadas foram caligrafia, estampagem, serigrafia e spray *coating*. A partir das análises estruturais por DRX, refinamento de Rietveld, MET e FTIR, foi possível identificar a formação da fase de interesse $GdAlO_3$, com estrutura perovskita ortorrômbica de grupo espacial *Pbnm*, além de confirmar a modificação superficial dos luminóforos com SiO_2. No que se refere à caracterização espectroscópica, medidas de fotoluminescência confirmaram emissões em diferentes regiões do visível (vermelho e verde) para os luminóforos e as tintas, sob distintas fontes de excitação (UV e IV, respectivamente), evidenciando o caráter dual dos materiais produzidos. Medidas de tempo de vida indicaram comportamento biexponencial nos sistemas downshifting (1,18-2,51 ms) e monoexponencial nos upconversion, com redução de 0,40 para 0,040 ms com o aumento da concentração de Yb^{3+}. O maior Φ_{Eu}^{L} (66,9%) foi observado para GAP5Eu, enquanto Φ_{Eu}^{Eu} atingiu 50,1% para GAP1Eu (λ_{exc} = 263 nm). A modificação com SiO_2 promoveu supressão da luminescência, evidenciada pela queda do rendimento quântico. As tintas aplicadas por impressão em cédulas e diferentes tipos de papéis representam avanços para a área de antifalsificação e sistemas de segurança multifuncionais.

Palavras-chave: íons terras raras; plataformas multifuncionais; combustão da ureia.

ABSTRACT

Counterfeiting is considered a significant problem that directly impacts the global economy, such as coins, checks, banknotes, works of art, and documents may present vulnerabilities due to the need for specialized authentication. In this context, luminescent materials are considered ideal for this application, as they provide multicolored emission, a fast response time, and sensitivity to various external stimuli. Thus, the objective of this work was to develop dual-emission luminescent inks based on $GdAlO_3$ phosphors containing Eu^{3+} ions (downshifting, DS) or Er^{3+}/Yb^{3+} ions (upconversion, UC), modified or not with SiO_2, for application in anti-counterfeiting printing systems. The urea combustion method, a self-sustained and environmentally friendly approach, was employed for the synthesis of the phosphors, while the Stöber method was used for surface modification with SiO_2. Luminescent inks were formulated using two polymeric matrices: polyvinyl alcohol (PVA) and glycerol. The printing techniques evaluated included calligraphy, stamping, screen printing, and spray coating. Structural analyses by XRD, Rietveld refinement, TEM, and FTIR confirmed the formation of the target $GdAlO_3$ phase, with an orthorhombic perovskite structure (space group *Pbnm*), as well as the successful surface modification of the phosphors with SiO_2. Regarding spectroscopic characterization, photoluminescence measurements confirmed emissions in different visible regions (red and green) for the phosphors and inks, under different excitation sources (UV and IR, respectively), highlighting the dual nature of the produced materials. Lifetime measurements indicated biexponential behavior in downshifting systems (1.18-2.51 ms) and monoexponential behavior in upconversion systems, with a reduction from 0.40 to 0.040 ms with increasing Yb^{3+} concentration. The highest Φ_{Eu}^{L} (66.9%) was observed for GAP5Eu, while Φ_{Eu}^{Eu} reached 50.1% for GAP1Eu (λ_{exc} = 263 nm). Modification with SiO_2 promoted luminescence suppression, evidenced by the drop in quantum yield. Inks used in the printing of banknotes and diverse paper substrates constitute important advancements in anti-counterfeiting technologies and multifunctional security systems.

Keywords: rare earth ions; multifunctional platforms; urea combustion.

LIST OF FIGURES

LIST OF TABLES

LIST OF ABBREVIATIONS AND CODES

IoT	Internet of Things
ISC	Intersystem Crossing
VB	Valence Band
CB	Conduction Band
CTB	Charge Transfer Band
DC	Downconversion
DS	Downshifting
UC	Upconversion
ESA	Excited-state Absorption
ETU	Energy Transfer Upconversion
CUC	Cooperative Upconversion
CR	Cross-relaxation
PA	Photon Avalanche
EMU	Energy Migration-mediated Upconversion
QR	Quick Response
RFID	Radio Frequency Identification
PVA	Polyvinyl alcohol
GAG	Gadolinium aluminum garnet
GAP	Gadolinium aluminum perovskite
GAM	Gadolinium aluminum phase
LLuMeS	Laboratory of Luminescence in Materials and Sensors
SSL	Solid-state lighting
HAADF	High Angle Annular Dark Field
IEP	Isoelectric point
PdI	Polydispersity index

LIST OF SYMBOLS

Ln^{3+}	Trivalent lanthanide ions
S_0	Singlet ground state
S_2	Higher-energy singlet excited state
T_1	Excited triplet state
RE^{3+}	Trivalent rare-earths ions
RE^{2+}	Divalent rare-earth ions
$REAlO_3$	Rare-earth-containing perovskite-type aluminate
τ	Tolerance factor
D_r	Percentage variation
r_A	Ionic radius of Gd^{3+}
r_B	Ionic radius of Al^{3+}
r_X	Ionic radius of O^{2-}
r_d	Ionic radius of Ln^{3+}
$\bar{x}_{Gd-O}$	Average Gd−O bond distance
$\bar{x}_{Al-O}$	Average Al−O bond distance
D	Distortion index
E_g	Optical band gap
λ_{dom}	Dominant wavelength
Φ_{Eu}^{Eu}	Intrinsic quantum yield
$\langle\tau\rangle$	Mean lifetime
A_{rad}	Radiative decay rate
A_{nrad}	Non-radiative decay rate
Φ_{Eu}^{L}	Absolute quantum yield
Ω_λ	Experimental Judd-Ofelt intensity parameter

TABLE OF CONTENTS

1 INTRODUCTION

1.1 STATE-OF-THE-ART

Counterfeiting is a major global issue with direct and substantial economic impacts. By 2022, public losses attributed to counterfeit currency were estimated at approximately USD 80 million, while, in the United States, losses with counterfeit checks exceeded USD 20 billion[1]. Among the materials particularly vulnerable to counterfeiting are coins, checks, banknotes[2], works of art[3], official-documents[4], and the packaging of high-value goods[5], many of which require expert authentication. Consequently, the continuous technological advancement of counterfeiting techniques has driven growing interest in the development of detection and prevention strategies (anti-counterfeiting), which play an important role in ensuring economic stability and human security[1].

In this context, the development of multifunctional products has attracted increasing attention in recent years[6]. Broadly, such devices can be classified into two categories: (*i*) electronic devices, with applications in healthcare, the Internet of Things (IoT), and artificial intelligence (AI); and (*ii*) photonic devices. The latter category encompasses a wide range of applications, including solid-state lighting[7], photodynamic therapy, fluorescence imaging, sensing, plasmon resonance-based imaging, and security devices[8], and is particularly attractive for optical study when compared with purely electronic materials.

Historically, the study of light emission and propagation spans more than a century; however, major advances occurred in the 1960s with the advent of lasers. These developments catalyzed progress in fields such as linear and quantum optics, and medical physics, ultimately leading to the emergence of so-called “photonic materials”, which are designed to enable precise control over light generation and propagation[9]. More recently, efforts to tailor the optical properties of these materials toward multifunctionality have driven a significant increase in research on nanomaterials. Within this context, devices capable of detecting counterfeits have gained prominence among numerous applications, a trend that can be attributed to rapid technological development and increasing globalization[10].

With this growth, the anti-counterfeiting market has increasingly adopted a variety of materials and technologies aimed at information security and protection, including magnetic systems, plasma-based features, holograms, and luminescent materials[10]. Among these, luminescence-based approaches are considered particularly effective for cryptography

and anti-counterfeiting applications, as they combine several advantageous properties, such as multicolor emission, fast response times, emission lifetimes ranging from nanoseconds to milliseconds, tunable emission wavelengths, and multimodal luminescence activated by different external stimuli, including electrical excitation, light irradiation, and thermal input[11].

However, not all phosphors possess properties suitable for applications. In this context, the incorporation of trivalent lanthanide ions (Ln^{3+}) into luminescent materials has emerged an attractive strategy to overcome these limitations and enhance performance in anti-counterfeiting applications.

1.2 LUMINESCENCE

1.2.1 Rare-earth ions and luminescent materials

The phenomenon of luminescence can be defined as the emission of electromagnetic radiation arising from electronic transitions following the excitation of electrons by an external stimulus, distinguishing it from incandescence, which is driven by thermal processes[12,13]. A wide range of materials exhibit light emission in the visible region, while in some cases emission can also occur in the ultraviolet (UV) and/or infrared (IR) regions, depending on the nature of the luminescent material[14].

Luminescence can be classified in several ways, one of which is based on the nature of the excitation source. Among these, photoluminescence (PL) refers to the emission of photons following electronic excitation by incident light, typically in the UV-Vis region. Photoluminescence can be further subdivided, particularly in systems containing organic chromophores, into fluorescence or phosphorescence, which arise from spin-allowed and spin-forbidden transitions, respectively[13]. **Figure 1** schematically presents the main luminescence classifications according to excitation source, along with a simplified Jablonski energy diagram illustrating excitation and relaxation pathways in which singlet and triplet states play a central role in the luminescence process.

Fluorescence, in turn, is a spin-allowed radiative process characterized by a short emission lifetime, typically in the range of 10^{-10} to 10^{-7} s. In this process, the material absorbs radiation in the UV or visible region and subsequently emits at a longer wavelength, a phenomenon known as the Stokes shift. Photoexcitation promotes an electron from the singlet ground state (S_0) to a higher-energy singlet excited state (e.g., S_2). This is followed by nonradiative processes, such as vibrational relaxation and internal conversion, which populate

lower-energy excited singlet states. Finally, the electron returns radiatively to the ground state S_0, and the time associated with this transition corresponds to the fluorescence lifetime, which is considered practically instantaneous relative to the excitation process[15].

In contrast, phosphorescent materials exhibit a spin-forbidden radiative process characterized by long emission lifetimes, typically ranging from 10^{-6} to 1 s. In this case, photon re-emission is slow and can persist even after the excitation source is removed. Phosphorescence arises from a spin-forbidden transition between the lowest excited triplet state (T_1) and the singlet ground state (S_0). Following initial photoexcitation, intersystem crossing (ISC) populates triplet state from an excited singlet state. The intrinsically low probability of the $T_1 \rightarrow S_0$ transition results in slow radiative decay and long-lived emission[16].

Figure 1. Types of luminescence according to different excitation sources and schematic representation of fluorescence and phosphorescence using the Jablonski energy diagram.

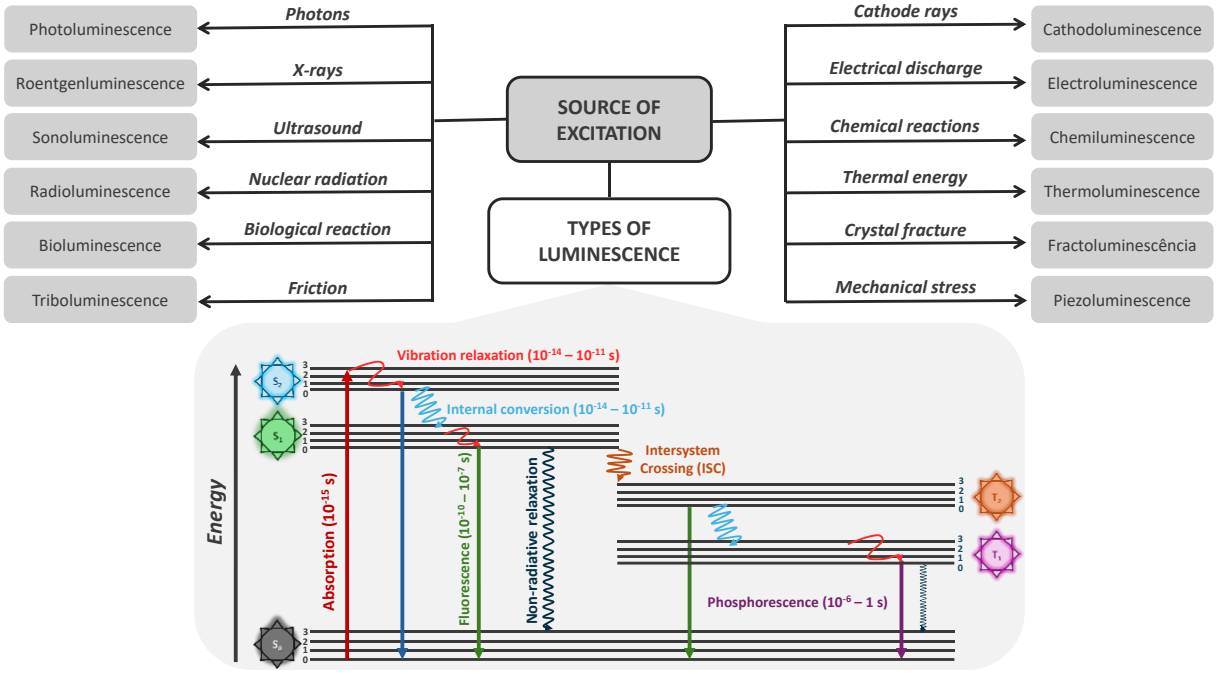

Source: Adapted from [14].

In photoluminescence (PL), particularly in the context of inorganic solids, the emission behavior depends on the absorption process, the nature of the host matrix, and the presence of an activator ion. Consequently, semiconductor materials are often preferred, as they possess a well-defined energy band gap between the valence band (VB) and the conduction band (CB), which is an essential condition for the occurrence of photoluminescence[17].

Thus, solids can exhibit intrinsic luminescence, which arises from radiative emission associated with the material's inherent electronic structure, without the

involvement of impurities or activating centers. This process typically occurs through the recombination of electron-hole pairs generated upon excitation or via emission from excitonic states, such that the emitted energy directly reflects the band gap or energy levels close to it. In contrast, extrinsic luminescence originates from structural defects or dopant ions that introduce additional levels in the band gap. This distinction is fundamental for understanding the emission mechanisms in inorganic and semiconductor materials[18].

With respect to extrinsic luminescence, this phenomenon is typically associated with an inorganic host matrix (H) doped with a controlled concentration of activating ions (A), and, in some cases, sensitizers. Among the most prominent activators are trivalent rare-earths (RE^{3+}), which comprise the lanthanide series (Ln^{3+}) as well as scandium (Sc^{3+}) and yttrium (Y^{3+}). In addition to rare-earth-based systems, several inorganic solids doped with transition metal ions also exhibit remarkable optical properties; classic examples include ZnS:Cu^{+} [19], ZnO:Co^{2+} [20], and $MgAl_2O_4$:Mn^{2+} [21]. In these materials, transition metal ions introduce electronic states within the band gap of the host lattice, enabling characteristic radiative emissions from dopant centers. **Figure 2** schematically illustrates the incorporation of an activating ion into an inorganic host matrix, commonly referred to as a phosphor.

Figure 2. Schematic representation of the host matrix (H) and doping with an Ln^{3+} type activator ion (A).

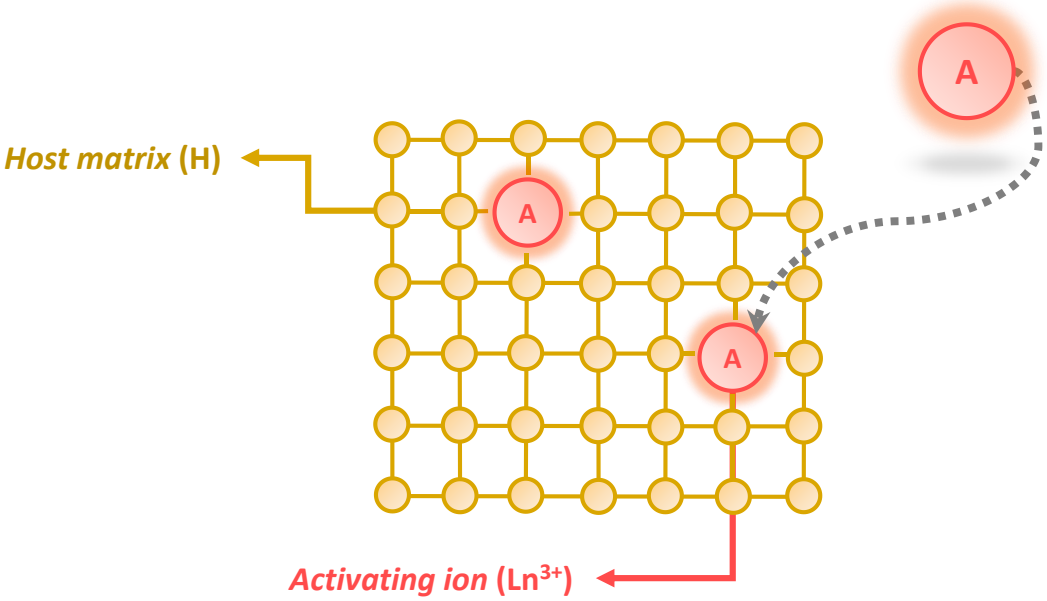

Source: Prepared by the author.

The incorporation of rare-earth ions confers significant advantages to this class of materials, including high emission efficiency, characteristic spectral profiles, and narrow, well-defined emission bands. As a result, rare-earth–based luminescent materials have found

important applications in photonics, such as temperature sensing, lasers, solid-state lighting, bioanalysis, medical therapy, and, more recently, in the expanding fields of anti-counterfeiting and forensic science[22].

The luminescence of trivalent lanthanide ions arises predominantly from electronic transitions within the 4*f* shell, which are formally parity-forbidden according to Laporte's selection rule. A distinctive feature of lanthanide ions from Ce^{3+} to Yb^{3+}, except for La^{3+} and Lu^{3+}, which possess empty and fully filled 4*f* shells, respectively, is that their optical properties originate from a partially filled 4*f* shell. The electrons in these orbitals are effectively shielded by the outer 5*s* and 5*p* shells, rendering them largely insensitive to the surrounding chemical environment. As a result, the energies of the 4*f*-derived electronic levels are only weakly perturbed by the host matrix[23]. The energy levels arising from the $4f^n$ electronic configurations of RE^{3+} ions were systematically investigated by Dieke[24] and later refined by Carnall and co-workers[25]. A partial energy-level diagram illustrating these states is shown in **Figure 3**.

Figure 3. Partial energy-level diagram of trivalent lanthanide ions (Ln^{3+}), showing the electronic states arising from the $4f^n$ configurations of Ln^{3+} and the main optical transitions in $LaCl_3$ host.

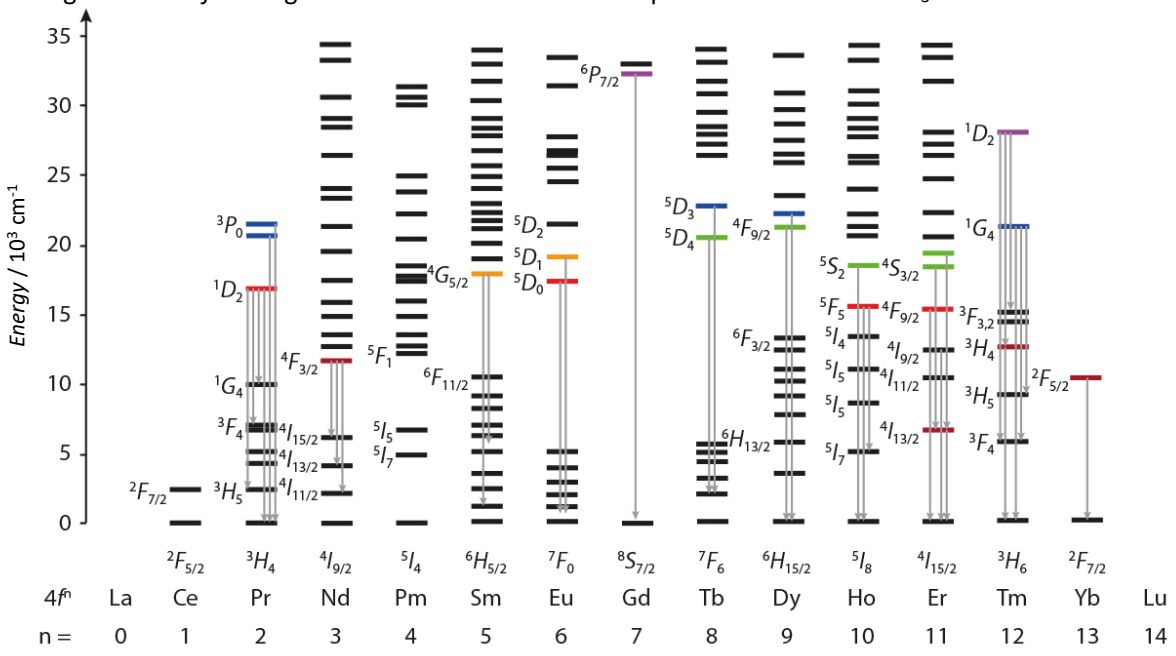

Source: Adapted from [26].

Phosphors doped or co-doped with Ln^{3+} can exhibit three distinct types of luminescent behavior: (*i*) narrow spectral bands arising from 4*f*-4*f* electronic transitions, which are formally forbidden by the Laporte selection rule; (*ii*) broad, crystal-field-dependent emission bands associated with 4*f*-5*d* type transitions, which are Laporte-allowed; and (*iii*)

charge transfer (CT) transitions, which also give rise to broad and intense bands and are likewise Laporte-allowed[13].

In *f-f* type electronic transitions, multiple 4*f* energy levels are typically observed for RE^{3+} ions, except for Ce^{3+} and Yb^{3+}, which possess only a single occupied or empty 4*f* level, respectively. Consequently, these transitions generally occur in the visible and infrared regions. In contrast, for Gd^{3+} ions, the *f-f* transition lies in the UV region due to the $4f^7$ electronic configuration, which gives rise to a highly stable $^8S_{7/2}$ ground state and the absence of low-energy excited 4*f* levels. These intraconfigurational *f-f* electronic transitions are electric dipole in nature and are strictly forbidden by Laporte's selection rule, as no change in parity occurs during the transition. However, this restriction can be partially relaxed when the activator ion incorporated into the host lattice site lacking an inversion center, which enables mixing of opposite-parity states and renders the transitions weakly allowed[14].

In *f-d* type transitions, an electron is promoted from a 4*f* level to a higher-energy 5*d* orbital. Unlike *f-f* transitions, these interconfigurational $f^n \rightarrow f^{n-1}d$ transitions are allowed by Laporte's selection rule. They are typically observed in rare-earth ions with a greater tendency towards oxidation, such as Sm^{2+}, Eu^{2+}, Yb^{2+}, Ce^{3+}, and Pr^{3+}. These divalent (RE^{2+}) and trivalent (RE^{3+}) ions in solids generally exhibit two main characteristics. The first is the presence of a broad emission band, arising from the strong interaction of the 5*d* orbitals with the chemical environment, which leads to significant crystal-field splitting of the 5d levels. The second is that 5*d*-4*f* transitions are electric-dipole allowed and can therefore be up to 10^6 times more intense than *f-f* transitions. A classic example is the YAG:Ce^{3+} phosphor, which is widely used in solid-state lighting and scintillator applications[27].

Charger transfer transitions correspond to redox processes in which an electron is promoted from neighboring atoms or ions to the 4*f* orbitals of the rare-earth ion. These interconfigurational transitions are fully allowed by selection rules, resulting in broad excitation bands commonly referred to charge transfer bands (CT). This type of transition is characteristic of more easily reducible RE^{3+} ions, such as Sm^{3+} and Eu^{3+}, as well as rare-earth species in higher oxidation states, including Ce^{4+}, Pr^{4+}, and Tb^{4+}. A classic example is the red-emitting phosphor Y_2O_3:Eu^{3+}. In this system, UV radiation excites the host lattice, composed of oxide ions (O^{2-}), which rapidly transfer the absorbed energy to the Eu^{3+} activator. This process corresponds to a ligand-to-metal charge transfer transition, commonly described by the reaction $O^{2-} \rightarrow Eu^{3+}$ [28].

1.2.2 Upconversion and downshifting process

In 1957, Dexter introduced the concept of splitting the energy of an UV photon into two lower-energy photons in the visible region of the electromagnetic spectrum. In this process, the energy of a high-frequency photon is efficiently converted into a pair of low-frequency photons[29]. This proposal gave rise to what is now known as downconversion (DC), also referred to in the literature as *quantum cutting*. This phenomenon is considered the inverse of upconversion[30], which is described in the following sections.

Similarly, the linear Stokes-type optical process known as downshifting (DS) involves the absorption of high-energy photons (shorter wavelength, in the UV or blue region) by a luminescent material, followed by the emission of lower-energy photons (longer wavelengths), typically in the visible region. The main difference between DS and DC lies in the photon balance: in DS, each absorbed photon results in the emission of only one photon, whereas in DC the absorption of a single photon can lead to the emission of two or more photons[30]. This contrast is schematically illustrated in **Figure 4**.

Figure 4. Simplified energy diagram for downconversion (DC) and downshifting (DS) processes.

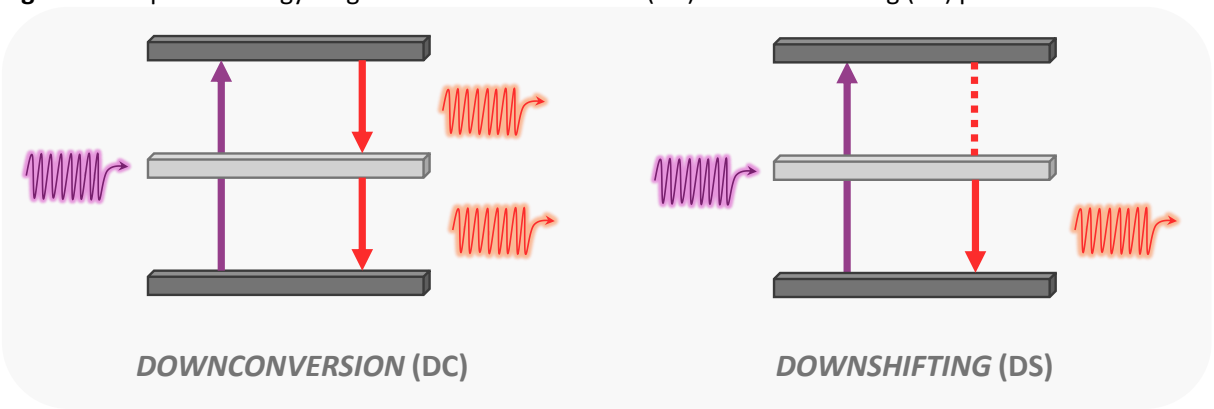

Source: Adapted from [26].

Materials exhibiting DS properties find applications in areas such as lasers, solar cells, bioimaging, and anti-counterfeiting technologies. The use of Ln^{3+} emitting ions, such as Eu^{3+}, is particularly advantageous in this process due to their high quantum efficiency. This efficiency is directly associated with the large energy separation between the excited and emitting states, which favors intense emission in the red of the visible spectrum[31], as illustrated by the energy-level scheme in the Dieke diagram, **Figure 3**.

Upconversion (UC) processes, particularly in lanthanide-based systems, are characterized as nonlinear anti-Stokes optical phenomena in which two or more near-infrared photons are sequentially absorbed via intermediate energy levels of Ln^{3+} ions, resulting in

emission at wavelengths shorter than those of the incident radiation, typically in the visible region of the spectrum[14]. Since the discovery of this phenomenon by Auzel[32] in the 1960s, extensive research has been carried out owing to its favorable optical characteristics, such as tunable emission profiles and a broad range of applications, including anti-counterfeiting technologies [33]. **Figure 5** schematically illustrates a UC.

Figure 5. Upconversion nanoparticle exhibiting anti-Stokes emission, in which the energy of the emitted photon is higher than that of the excitation photon ($\lambda_{ex}>\lambda_{em}$) (a) and simplified energy-level diagram showing perturbations arising from the Coulomb interaction (H_c), spin-orbital coupling (H_{so}), and crystal field interaction (H_{cf}) (b).

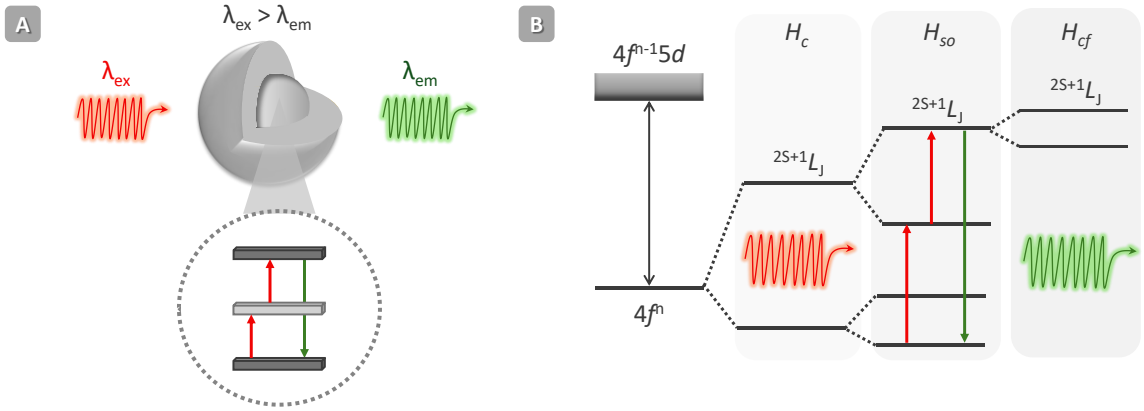

Source: Adapted from [34].

To evaluate the efficiency of these devices, various upconversion mechanisms in lanthanide-doped systems have been investigated and are generally classified into six types: (*i*) excited-state absorption (ESA); (*ii*) energy transfer upconversion (ETU); (*iii*) cooperative upconversion (CUC); (*iv*) cross-relaxation (CR); (*v*) photon avalanche (PA); and (*vi*) energy migration-mediated upconversion (EMU)[34]. Each of these processes is schematically illustrated in **Figure 6**.

Figure 6. Main upconversion mechanisms of nanomaterials doped with lanthanide ions. ESA, ETU, EMU, CUC, CR, and PA represent excited-state absorption, upconversion energy transfer, cooperative upconversion, cross-relaxation, and photon avalanche, respectively.

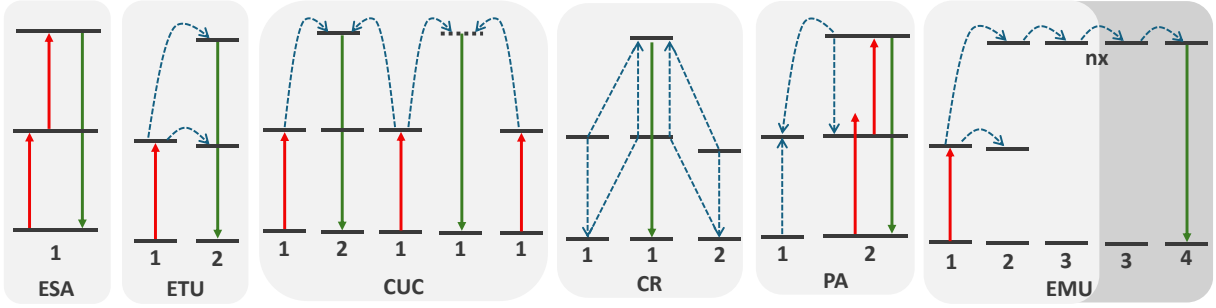

Source: Adapted from [34].

In the ESA mechanism, the successive absorption of photons by the same ion (1), **Figure 6**, promotes electronic transitions from the ground state to higher-energy excited states. For the process to be efficient, the energy levels of the Ln^{3+} ions must exhibit a 'staircase' arrangement with approximately uniform spacing. Ions such as Ho^{3+}, Er^{3+}, and Tm^{3+} are classic examples of luminescence centers well suited for triggering the ESA-based upconversion mechanisms[34].

Similarly to the ESA mechanism, the ETU process also involves the sequential absorption of photons leading to the population of intermediate levels of the lanthanide dopant ions. However, unlike ESA, ETU requires interactions between two distinct types of ions in the host matrix: the sensitizer (1) and the activator (2). In this context, Yb^{3+} is widely employed as a sensitizer due to its large absorption cross-section at 980 nm, which coincides with the emission wavelength of commercially available diode lasers. Furthermore, the efficiency of the ETU critically depends on the average distance between sensitizer and activator ions, which is directly governed by their doping concentrations[34].

The CUC mechanism is a three- or four-body process in which the population of emitting levels occurs through cooperative energy transfer between adjacent ions. This mechanism generally encompasses two related phenomena: cooperative luminescence and cooperative sensitization. In cooperative luminescence, both the energy donor (1) and the acceptor (2) correspond to the same lanthanide ion, as exemplified by Yb^{3+}-Yb^{3+} pairs. In contrast, cooperative sensitization involves different lanthanide ions, such as in the Yb^{3+}-Eu^{3+} pairs[34].

The CR process corresponds to an energy-transfer interaction occurring between activator ions of the same type (1 and 1) or of different types (1 and 2), provided that their optical transitions are energetically resonant. In addition to being recognized as one of the primary main causes of concentration quenching, cross-relaxation can also be intentionally exploited to modulate and tailor emission profiles. A representative example is the incorporation of Ce^{3+} into Yb^{3+}-Ho^{3+}-doped materials, where CR between Ho^{3+} and Ce^{3+} ions is used to tune the upconversion emission of Ho^{3+} from green to red[34].

In the case of PA, excitation intensities above a certain threshold are required. The essential conditions for triggering this process include weak ground-state absorption, strong excited-state absorption, and efficient cross-relaxation pathways. Owing to the positive

feedback between excited-state absorption and cross-relaxation, the PA mechanism can exhibit particularly high upconversion efficiency[34].

Finally, the EMU mechanism requires four distinct types of lanthanide dopants arranged within a core@shell architecture. In this process, a primary sensitizing ion (1) absorbs excitation photons in the near-infrared region and sequentially transfers its excitation energy to an accumulator ion (2). Subsequently, a migrating ion (3), typically Gd^{3+}, accepts energy from the accumulator at neighboring sites, enabling random energy hopping throughout the core@shell structure. Ultimately, an activating ion (4) captures this migrating energy and generates upconversion emissions. The core@shell architecture and the controlled spatial distribution of the dopants provide significant advantages by minimizing luminescence quenching and facilitating energy transfer between the accumulator and activator, an essential step for achieving high EMU efficiency[34].

1.2.3 Luminescence of Eu^{3+}, Gd^{3+}, and Er^{3+}/Yb^{3+} ions

A luminescent center incorporated into a host matrix is referred to as a dopant or activator ion. In inorganic solids, these ions are responsible for the characteristic electronic and optical properties of phosphors. In addition to activators, certain ions can act as sensitizers or co-dopants by absorbing excitation energy and transferring it to the activator ions. RE ions can exhibit oxidation states ranging from 2+ to 4+, with the trivalent state (3+) being the most prevalent, owing to the enhanced stability of their electronic configuration[15].

Table 1 summarizes the main characteristics of the rare earth ions investigated in this work: Gd^{3+}, used as a constituent cation of the host matrix; Eu^{3+}, associated with downshifting processes, and the Er^{3+}/Yb^{3+} pair, which exhibits upconversion properties. It is noteworthy that the initial concept of the project also included the use of Tb^{3+} as a downshifting activator ion emitting in the green region. However, due to the weak emission intensity observed in the resulting phosphors, the material formulation strategy was subsequently modified.

Table 1. Atomic and spectroscopic parameters of the RE^{3+} ions studied in this work, including atomic number (Z), electronic configuration, hypersensitive transitions, and associated emitting levels and luminescence processes.

Element – Z	Electronic configuration	RE^{3+} configuration	Hypersensitive transition		Excited emission level	Process
			Excited state	Fundamental state		
Eu – 63	$[Xe]4f^7 6s^2$	$[Xe]4f^6$	$^7F_2$	$^7F_1$ $^7F_0$	$^5D_0$	DS
Gd – 64	$[Xe]4f^7 5d^1 6s^2$	$[Xe]4f^7$	-	$^8S_{7/2}$	-	ET
Er – 68	$[Xe]4f^{12} 6s^2$	$[Xe]4f^{11}$	$^2H_{11/2}$ $^4G_{11/2}$	$^4I_{15/2}$	$^4I_{13/2}$	DS and UC
Yb – 70	$[Xe]4f^{14} 6s^2$	$[Xe]4f^{13}$	-	-	$^2F_{5/2}$	UC

DS = downshifting; UC = upconversion; ET = energy transfer
Source: Adapted from [14].

The europium(III) ion exhibits well-defined and highly characteristic spectroscopic properties. Based on its electronic configuration, $[Xe]4f^6$, the six electrons distributed among the seven 4*f* orbitals can combine to form 3,003 microstates. Because these electrons occupy inner 4*f* orbitals close to the nucleus, they are effectively screened from crystal-field perturbations by the filled 5*s* and 5*p* orbitals. Intrinsic electromagnetic interactions within the ion lift the degeneracy of the 4*f* orbitals, giving rise to multiple discrete energy levels responsible for optical transitions primarily in the red and near-infrared regions. Consequently, when incorporated into an inorganic host matrix, the energetic positions of the Eu^{3+} emission bands are only weakly influenced by the surrounding lattice, resulting in narrow emission bands in the orange-to-red spectral range (580-720 nm). This combination of spectral stability and sharp emission bands underpins the widespread use of Eu^{3+} in high-performance optical devices and anti-counterfeiting applications[35].

The 4*f*-4*f* electronic transitions of Eu^{3+} exhibit low molar absorptivity when the ion occupies centrosymmetric environments, due to the prohibition imposed by the Laporte selection rule. Furthermore, the spectral profile, Stark splitting, and relative intensities of the bands composing the Eu^{3+} emission spectrum are highly sensitive to the local symmetry, both in inorganic solids and in molecular complexes. This sensitivity makes Eu^{3+} not only an efficient red-emitting ion but also a valuable structural probe for assessing the local environment in inorganic host matrices[36].

Regarding the main emissions observed in the visible region, the transitions originating from the excited level $^5D_0$ to the lower-lying $^7F_{0\text{-}6}$ levels (J=0-6), denoted as $^5D_0 \rightarrow {}^7F_J$, are the most prominent. Emissions arising from the higher excited states $^5D_1$ and $^5D_2$ may also

be observed under appropriate excitation conditions. Among these transitions, the $^5D_0 \rightarrow {}^7F_2$ transition, centered around 612 nm, is particularly significant, as it is governed by a forced electric dipole mechanism. This transition typically exhibits the highest relative intensity in crystalline solids where Eu^{3+} occupies low-symmetry sites lacking an inversion center. For this reason, it is termed a "hypersensitive" transition, as it strongly reflects variations in the local chemical environment surrounding Eu^{3+} ion[36]. **Table 2** provides a general description of the transitions observed in the emission spectra of europium(III) compounds.

Table 2. Description of the electronic transitions observed in the emission spectra of the Eu^{3+} ion.

Transition	λ interval / nm	Mechanism	Characteristics
$^5D_0 \rightarrow {}^7F_0$	570-585	Electric dipole (ED) and magnetic dipole (MD) forbidden. Occurs due to J mixing	Observed only in C_n, C_{nv}, and C_s symmetries and exhibits, at most, one Stark component (2J+1) for each site lacking an inversion center. The relaxation of the selection rules arises from the mixing of J=2, 4, and 6 states.
$^5D_0 \rightarrow {}^7F_1$	585-600	Magnetic-dipole allowed	Low sensitivity to the chemical environment and presents a limited number of Stark components. When Eu^{3+} ions occupy sites lacking an inversion center, a noticeable increase in emission intensity is observed.
$^5D_0 \rightarrow {}^7F_2$	610-630	Induced electric-dipole allowed	"Hypersensitive" transition exhibiting enhanced intensity in inorganic solids when Eu^{3+} occupies sites lacking an inversion center, with up to five Stark components and high sensitivity to the local chemical environment.
$^5D_0 \rightarrow {}^7F_3$	640-660	Forbidden. Occurs due to J mixing	May exhibit up to seven Stark components in the emission spectrum and generally displays low emission intensity.
$^5D_0 \rightarrow {}^7F_4$	680-710	Induced electric-dipole allowed	This transition tends to increase in intensity with increasing site symmetry and can exhibit up to nine Stark components per site.

Source: Adapted from [36].

The Gd^{3+} cation, which has the configuration [Xe]$4f^7$, has well-established optical and magnetic properties, first systematically investigated in the late 19th century following the isolation of gadolinium by Jean Charles de Marigna in 1880. From the energy level diagram of Gd^{3+}, (**Figure 7)**, it can be inferred that upon energy absorption, the ion can be excited from the $^8S_{7/2}$ state to higher-lying levels such as the ^6P_J manifold, followed by further excitation to more energetic states. Subsequently, non-radiative relaxation may occur to lower excited states, such as the ^6I_J manifold, before returning to the $^8S_{7/2}$ ground state[37].

With respect to the spectroscopic properties of the activator/sensitizer pair Er^{3+} [Xe]$4f^{11}$ and Yb^{3+} [Xe]$4f^{13}$, Yb^{3+} is widely employed as an efficient sensitizer for Er^{3+}, particularly

under near-infrared excitation around 980 nm. In this excitation scheme, only the $^2F_{7/2} \rightarrow {}^2F_{5/2}$ transition of Yb^{3+} is involved, since this ion possesses a single excited multiplet associated with its $4f^{13}$ electronic configuration. This transition is spin-allowed, as no change in spin multiplicity occurs. When incorporated into an inorganic host matrix, the excited $^2F_{5/2}$ state of Yb^{3+} can split into up to three Stark sublevels, while the ground $^2F_{7/2}$ state can split into up to four sublevels, in accordance with the Kramers splitting rule for ions with an odd number of 4*f* electrons, (J+1/2 degeneracy)[38].

The Er^{3+} exhibits multiple excited energy levels, whose sensitization can give rise to different emission bands. Among these, the $^4H_{11/2}, {}^4S_{3/2} \rightarrow {}^4I_{15/2}$ and $^4F_{9/2} \rightarrow {}^4I_{15/2}$ transitions stand out, being responsible for green and red emissions, respectively, and are the most frequently observed. However, the small energy gaps between the Er^{3+} excited states favor non-radiative relaxation processes, which reduce the emission quantum yield via multiphonon relaxation. Therefore, to suppress this deactivation pathway, Er^{3+} ions should be incorporated into matrices with low phonon energies[39].

Strategically, in this work, the combination of the Eu^{3+}, associated with the DS process, and the Yb^{3+}/Er^{3+} pair, associated with the UC, enables the development of materials with a “dual” optical functionality. These materials can exhibit distinct emission responses under different excitation sources namely UV and near-infrared irradiation, respectively. **Figure 7** shows simplified energy-level diagrams of the Ln^{3+} ions investigated in this study, highlighting the main electronic transitions involved.

Figure 7. Simplified energy-level diagrams of Gd^{3+}, Eu^{3+}, Er^{3+}, and Yb^{3+} ions.

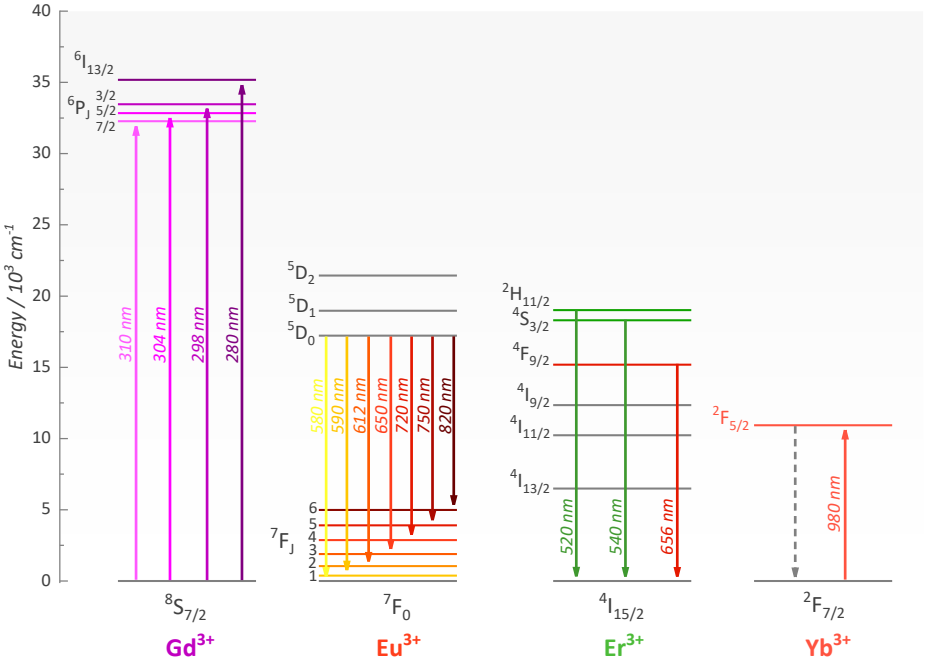

Source: Prepared by the author.

1.3 LUMINESCENT INKS APPLICABLE IN ANTI-COUNTERFEITING

Within the area of anti-counterfeiting, several technologies have been developed to prevent fraud, particularly in high value-added products. However, commonly employed approaches, such as (*i*) Quick Response (QR) codes[40]; (*ii*) Radio Frequency Identification (RFID)[41]; (*iii*) security labels based on plasmonic technology[42]; and (*iv*) holograms[43], present notable limitations. These include the requirement for specialized manufacturing equipment, the use of potentially toxic chemicals, and the overall complexity of fabrication and implementation procedures[44].

As a promising alternative, luminescent nanomaterials doped with lanthanide ions and employed as security inks have attracted significant attention in recent years. These materials have become well established as effective tools for security markings, authentication labels, barcode systems, and QR codes. Their main advantages include well-defined emission bands, long operational lifetime, chemical and thermal stability, high solubility, low toxicity, ease of preparation, and high performance in security and anti-counterfeiting applications[45].

The production of fluorescent security patterns using luminescent inks requires careful consideration of several key elements, including the selection of the dispersing matrix, usually an organic polymer, gel, colloid, or solid powder; the choice of the phosphor to be

incorporated; the application substrate; and the printing method. The durability of the resulting ink is influenced by both the printing technique employed and the adhesion of the luminescent material to the substrate, which depends on the substrate nature (porous or non-porous) and consequently determines its resistance to deterioration. Print resolution is also a critical factor, as patterns with higher definition tend to exhibit greater durability. In addition, the visibility of the printed features can be affected by the viewing angle and the contrast of the pattern. Therefore, parameters such as cost, manufacturing speed, and environmental conditions are key considerations in the design and implementation of these materials[45].

Printing technologies can be broadly classified into two categories: contact and contactless methods. In contact-based techniques, such as calligraphy and stamping, printing occurs through direct physical contact between the substrate and predefined structures previously impregnated with ink. In the present work, screen printing represents a contact method, whereas spray coating is classified as a contactless technique. In these cases, the ink solution or suspension is atomized and dispersed through nozzles, while the desired patterns are formed on the substrate by controlled movement of the spray head or the substrate holder according to a pre-programmed design[46].

The calligraphy (handwriting) method is regarded as the oldest and simplest technique for producing signatures, characters, patterns or phrases on paper documents, using pens filled with anti-counterfeiting inks. It is particularly effective for rapid testing with high viscosity inks, which are generally unsuitable for contactless printing technologies. This method is widely employed in the manufacture of security pens containing invisible inks used in official documents, where the written signature becomes visible only upon exposure to an external stimulus, such as UV and/or IR excitation. In this approach, the ink viscosity must be higher than required for inkjet printing, for example. Such an increase in viscosity can be achieved by incorporating high molecular-weight polymers, such as polyvinyl alcohol PVA or glycerol in water-based inks, and acrylic polymers in solvent-based formulations[47].

Stamping is a contact printing technique commonly used to apply predefined patterns to documents on various types of paper using medium-viscosity anti-counterfeiting inks. It is a fast and straightforward method, capable of producing a wide range of security patterns or marks within a short time. A variety of polymers can be employed in the formulation of these inks, and the addition of volatile organic solvents, such as ethanol, is

often used to accelerate the drying process. Both stamps and pens are portable tools, enabling rapid and practical security marking of documents[48].

Among contactless printing technologies, screen printing is regarded as one of the oldest techniques for depositing high-viscosity inks onto a wide variety of substrates. In this method, the ink is forced through the patterned mesh of a screen by a shear force applied parallel to the substrate surface, typically generated by the operator using a squeegee. As a result, discrete ink droplets are transferred onto the substrate positioned beneath the screen. The mesh size is the primary factor determining the resolution of the printed patterns, with finer meshes enabling higher printing resolution[49].

Finally, the spray coating method is based on the deposition of ink through a gas-driven spray, requiring formulations of relatively lower viscosity to prevent nozzle clogging. In this process, the atomized ink is directed onto the substrate, where solvent evaporation, promoted by heating or ambient airflow, leads to the formation of a continuous coating layer. The quality of the resulting coating can be assessed in terms of phase stability, coating density (i.e., the number of deposited layers) and the degree of ink absorption by the substrate. As its main advantages, spray coating allows the use of a wide variety of inks formulations and is compatible with diverse substrate types[50]. **Table 3** summarizes the printing methods employed in this work, along with their respective advantages.

Table 3. Summary of printing technologies, methods, and associated advantages for luminescent anti-counterfeiting inks.

Technology	Printing method	Advantages
Contact printing	Calligraphy	- Easy to perform. - Efficient for quick tests. - Invisible ink signature. - Operates with high viscosity. - Portable.
	Stamping	- Pre-established patterns. - Operation on different substrates. - Quick and easy printing. - Short run time. - Compatibility with different solvents. - Portable.
Contactless printing	Screen printing	- Most traditional and one of the most reported methods. - Versatility in mesh selection. - High resolution in patterns.
	Spray coating	- Wide range of applications beyond anti-counterfeiting. - Works in different ink formulations. - Adhesion to numerous substrates.

Source: Adapted from [44].

1.4 GADOLINIUM ALUMINATE

In recent years, the market for luminescent materials doped with rare-earth ions has experienced steady growth. The incorporation of these ions into host matrices confers luminescent, physical and chemical properties of significant interest, marking this field particularly attractive to researchers[51].

Rare-earth-containing perovskite-type aluminates ($REAlO_3$) exhibit a wide range of technological applications, including their use as scintillators[52], optical lasers materials[53], and dielectrics[54]. Within the broader class of inorganic compounds, perovskites stand out as a particularly important and versatile category.

In the Gd_2O_3-Al_2O_3 system, three crystalline phases can be formed: the metastable gadolinium aluminum garnet (GAG, $Gd_3Al_5O_{12}$), the thermodynamically stable gadolinium aluminum perovskite (GAP, $GdAlO_3$), and monoclinic gadolinium aluminum phase (GAM, $Gd_4Al_2O_9$)[55,56]. These three phases are illustrated in **Figure 8.**

Figure 8. Possible crystalline phases in the Gd_2O_3-Al_2O_3 system: gadolinium aluminum garnet (GAG, $Gd_3Al_5O_{12}$) (a), stable gadolinium aluminum perovskite (GAP, $GdAlO_3$) (b), and monoclinic gadolinum aluminum phase (GAM, $Gd_4Al_2O_9$) (c). The crystal structures were constructed based on CIF data.

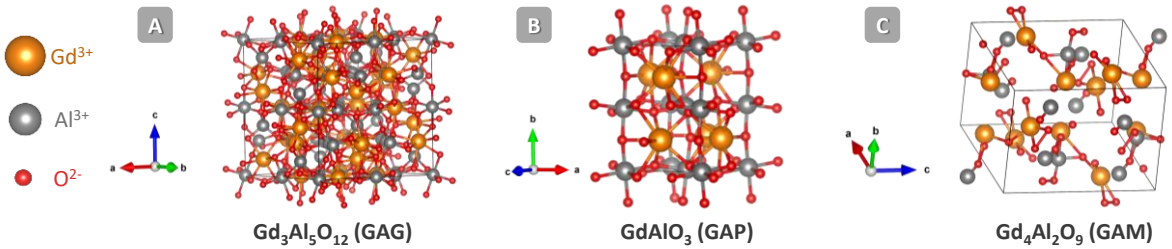

Source: Prepared by the author.

Among gadolinium-aluminum perovskites, the distorted perovskite phase with an orthorhombic crystal system ($GdAlO_3$) exhibit promising physical and chemical properties when doped with RE^{3+} ions. These characteristics make the material attractive for application across a wide range of fields, including scintillators[57], display technologies[58], neutron absorption in the petrochemical industry[59], oxygen-ion conduction,[60] and anti-counterfeiting technologies[61,62].

In GAP-type gadolinium aluminates, which crystallize in the orthorhombic space group *Pbnm*, Gd^{3+} ions occupy the A site of the ABO_3 lattice, where they are nominally surrounded by 12 O^{2-} anions, while each Al^{3+} ion occupies the B site and is coordinated by six O^{2-} anions, forming AlO_6 octahedra. However, due to the cooperative rotations and tilting of the AlO_6 octahedra characteristic of this orthorhombic structure, the 12-fold coordination

environment of Gd^{3+} becomes quite distorted and is more accurately described as eight shorter Gd-O bonds and four longer contacts (commonly denoted as “12=8+4”). In contrast, Al^{3+} ions retain a nearly ideal octahedral (sixfold) coordination by oxygens.

Upon incorporation of RE^{3+} dopant ions into this structure, substitution preferentially occurs at the Gd^{3+} sites, which possess C_s point symmetry, owing to the close similarity in ionic radii. In this environment, the dopant ions are effectively coordinated by eight oxygen atoms arranged in a distorted dodecahedron geometry[63]. **Figure 9** illustrates the crystal structure of the $GdAlO_3$ matrix, highlighting the Gd^{3+} and Al^{3+} sites with coordination numbers of 8 and 6, respectively.

Figure 9. Crystal structure of the orthorhombic $GdAlO_3$ perovskite matrix: overall structure (a); octacoordinated Gd^{3+} site (CN=8), exhibiting a dodecahedral coordination environment; hexacoordinated Al^{3+} site (CN=6), exhibiting an octahedral coordination geometry.

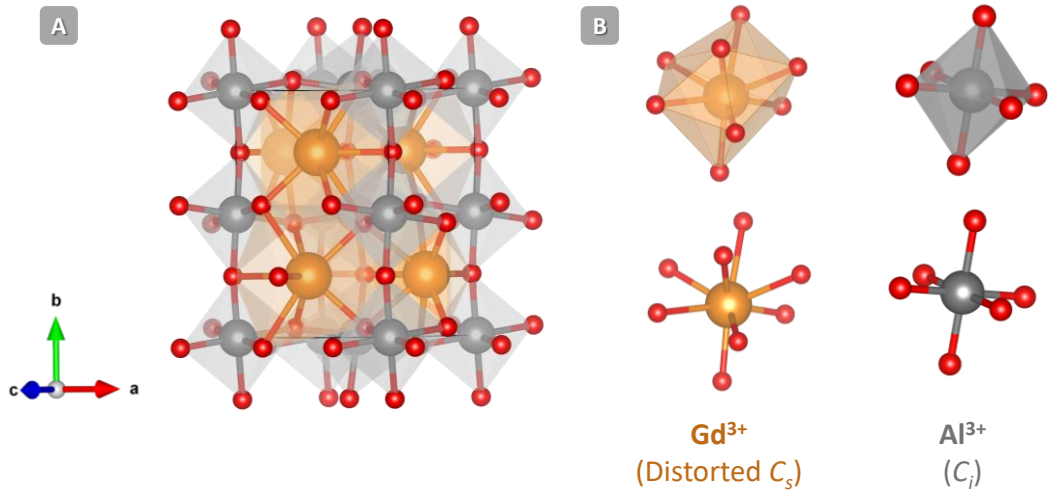

Source: Prepared by the author. Structures built using VESTA software and data from the CIF (Crystallographic Information File) code 2014561.

Table 4 presents the coordination numbers and corresponding ionic radius for the constituent ions of the host matrix, Gd^{3+}, Al^{3+}, and O^{2-}, as well as those of the dopant ions employed in this study: Eu^{3+} for downshifting applications and the Er^{3+}/Yb^{3+} pair for upconversion processes.

Table 4. Ionic radii of the constituent ions in the $GdAlO_3$ matrix and RE^{3+} dopant ions.

Ion	Coordination number	Ionic radius / pm	Ionic radius / Å
Gd^{3+}	6	94	0.94
	8	105	1.05
Al^{3+}	6	53	0.53
O^{2-}	6	140	1.40
	8	142	1.42
Eu^{3+}	6	95	0.95
	8	107	1.07
Er^{3+}	6	89	0.89
	8	100	1.00
Yb^{3+}	6	87	0.87
	8	99	0.99

Source: Adapted from [64]

The use of GAP-type aluminates as host matrices for rare-earth ions offers promising advantages for light emission across different spectral regions. In this context, materials based on the Gd_2O_3-Al_2O_3 system have been widely reported in the literature due to their chemical stability and favorable compatibility as hosts for a variety of activator ions[65,66,67,68].

Among perovskite-type materials, $GdAlO_3$ stands out due to its adequate structural stability and relatively low phonon energy (~580 cm^{-1})[69]. This feature makes it particularly suitable as a host matrix for upconversion materials, as non-radiative relaxation losses are significantly reduced during energy-transfer processes between sensitizers and activator ions, as well as during radiative decay pathways involved in downshifting processes[70].

Phase transition studies have shown that GAP undergoes a transformation from the orthorhombic phase to the rhombohedral phase at 1973 K. Furthermore, based on the estimates derived from the c/a lattice parameter ratio, which reflects the vertex distances of the unit cell, a continuous transition to the cubic phase was predicted at approximately 2580 K, a temperature higher than the melting point (2273 K)[71].

In addition to temperature effects, the literature also reports structural investigations under varying pressure conditions using single-crystal X-ray diffraction[72]. These studies revealed that the material remains isostructural over the investigated pressure range, even at pressures as high as 7.95 GPa. Furthermore, it was observed that the GdO_{12} polyhedral are less compressible than the AlO_6 octahedra, leading to an increase in the Al-O_1-Al and Al-O_2-Al bond angles with increasing pressure. This behavior indicates that GAP undergoes

only minor structural distortions, even under high pressure conditions, highlighting its robustness as a host matrix.

1.5 MODIFIED UREA COMBUSTION AND STÖBER METHOD

Experimental procedure exerts a significant influence on material performance. In this sense, the choice of the synthesis method for phosphors is crucial, as it governs several key properties, including microstructure, magnetic behavior, luminescent properties, and quantum efficiency[73]. In general, luminescent materials can be prepared through different synthetic routes, which may be broadly classified into two main categories: (*i*) solid-state reactions and (*ii*) solution-based syntheses.

In the solid-state reaction method, solid precursors corresponding to the constituent cations of the phosphors are employed. However, the formation of dense grains necessitates prolonged and high-temperature heat treatments during the calcination step to achieve the desired properties. Under these conditions, luminescent materials may undergo changes in their characteristics due to the volatility or chemical instability of their constituents[74].

To reduce the calcination temperature, the final material must exhibit smaller grains with a nanometric scale distribution. Accordingly, to achieve milder thermal conditions, enhanced morphological control, and lower energy consumption, phosphors such as GAP-type gadolinium aluminate have been preferentially prepared using various solution-based synthesis methods, among which the solution combustion method stands out as one of the most widely employed for this class of materials[75].

The combustion method is an example of a wet route that, in principle, does not require additional calcinations or repeated heating. Historically, this method was discovered accidentally in 1988 in India. It is based on a highly exothermic reaction that proceeds with the release of heat and light. The combustion of a homogeneous mixture of precursor solutions and fuel results in the formation of a voluminous, foamy phosphor. The flame temperature generated inside the furnace can be monitored using an optical pyrometer. Such high temperatures enable the rapid formation and crystallization of phosphors within a short time interval (3-12 minutes)[76].

Because it is a combustion-based process, a suitable combination of fuel and oxidant is required. For the synthesis of aluminates and/or oxides, metal nitrates are

preferentially employed as oxidants, while fuel sources typically include urea, hydrazine, or glycine-based compounds. The stoichiometric ratio between metal nitrates (O) and fuels (F) is commonly calculated using principles of propellant chemistry, which are widely applied in rocket and missile propulsion as well as in aerosol expulsion systems[76].

Thus, the maximum heat of combustion is achieved when the O/F ratio equals unity (O/F= 1). By convention, the elements C, H, V, B, or other metals are treated as reducing species, with assigned valences of 4+, 1+, 5+, 3+ (or the oxidation state of the metal ion in the corresponding compound), respectively. In contrast, for oxidizing species, oxygen is assigned to a valence of 2-, whereas nitrogen is considered to have a valence of zero, as it is converted to molecular nitrogen during the combustion step[76]. **Table 5** summarizes the oxidizing and reducing valences of the metal nitrates and fuels used in the synthesis of phosphors.

Table 5. Oxidizing and reducing valencies of metal nitrates and fuels, along with an example of valency calculation.

Compound	Oxidizing/Reducing valency	Example
$M(NO_3)_2$	10-	$M(NO_3)_3$ 1 M = 3+ 9 O = 18- 3 N = 0 Valency = 15-
$M(NO_3)_3$	15-	
$M(NO_3)_4$	20-	
NH_4NO_3	2-	
Urea, CH_4N_2O	6+	
Carbohydrazide (CH), $CH_6N_4O_2$	8+	
Oxalyl dihydrazide (ODH), $C_2H_6N_4O_2$	10+	CH_4N_2O 1 C = 4+ 4 H =4+ 2 N = 0 O = 2- Valency = 6+
3-Methyl Pyrazole 5-One (3MP5O), $C_4H_6N_2O$	20+	
Diformyl hydrazine (DFH), $C_2H_4N_2O_2$	8+	
$Y(N_2H_3COO)_3$	12+	
NH_4VO_3	3+	

Source: Adapted from [76].

However, for applications in the security field, the direct use of phosphors in powder form for the formulation of luminescent inks may be limited by the low solubility of materials produced via the combustion method. As an alternative, a widely adopted strategy involves coating the phosphors with SiO_2 to form core@shell systems. This approach enhances the hydrophilicity of the material with minimal interference in its luminescent properties, thereby enabling the preparation of stable suspensions suitable for security -related

applications. In addition, the silica shell provides surface protection by reducing direct contact between the phosphor and luminescence-quenching species[77].

The silica coating is based on the classic methodology proposed by Stöber, originally developed for the production and investigation of monodisperse colloidal suspensions of SiO_2 spheres[78]. The experimental procedure involves the formation of spherical particles through the hydrolysis of alkyl silicates (**Reaction 1**), followed by the condensation of silicic acid in an ethanolic medium (**Reaction 2**), with ammonia acting as a basic catalyst for the precursor reagents.

$$Si(OC_2H_5)_{4\ (aq)} + 4\ H_2O_{\ (l)} \longrightarrow Si(OH)_{4\ (aq)} + 4\ C_2H_5OH_{\ (aq)} \quad \textbf{(1)}$$

$$Si(OH)_{4\ (aq)} \longrightarrow SiO_{2\ (s)} + 2\ H_2O_{\ (l)} \quad \textbf{(2)}$$

Figure 10 illustrates the schematic representation of the steps in the process proposed by Stöber, adapted from the mechanism suggested for the hydrolysis of tetraethyl orthosilicate (TEOS).

Figure 10. Proposed mechanism for the hydrolysis of alkyl silicate in a basic medium.

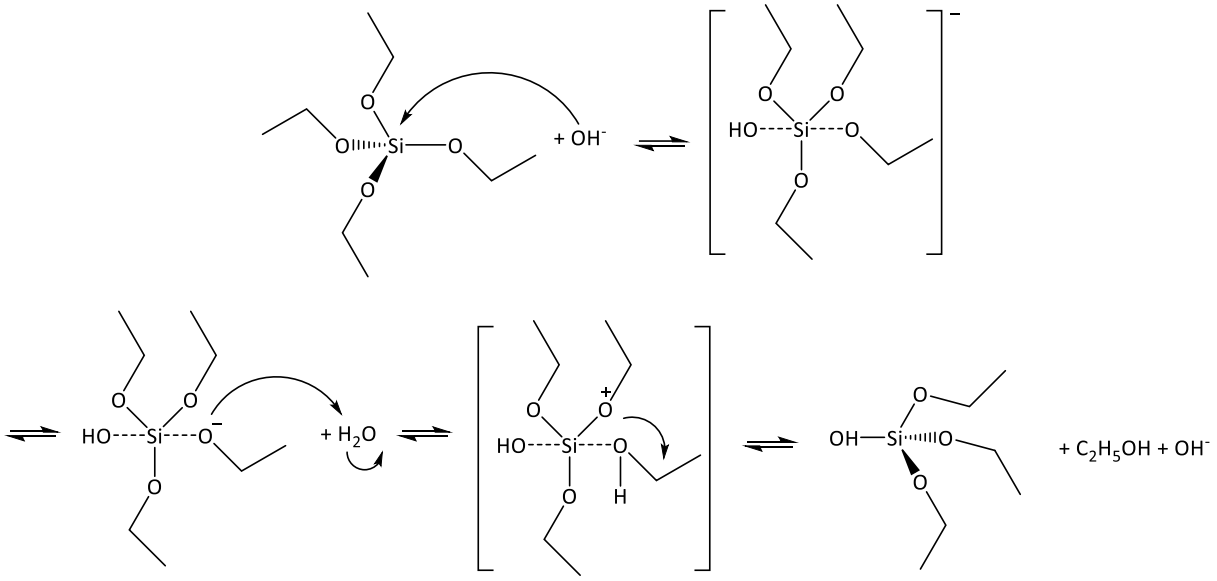

Source: Adapted from [78].

In the first step of the method, a nucleophilic attack by a hydroxyl ion occurs at the silicon atom of the TEOS precursor. The reaction leads to the formation of an anionic intermediate, in which the negatively charged oxygen subsequently promotes a nucleophilic attack on a water molecule present in the reaction medium. As a result, protonation takes place, followed by the departure of the leaving group, yielding the target intermediate for the subsequent steps through successive hydrolysis reactions. During this process, ethanol, originating from the leaving group, and hydroxide ions are generated and maintained in the

reaction medium by the action of the basic catalyst. **Figure 11** shows the proposed mechanism for the polycondensation reaction, which uses the hydrolysis-derived intermediate as precursor.

Figure 11. Proposed mechanism for the polycondensation reaction to form silica in a basic medium.

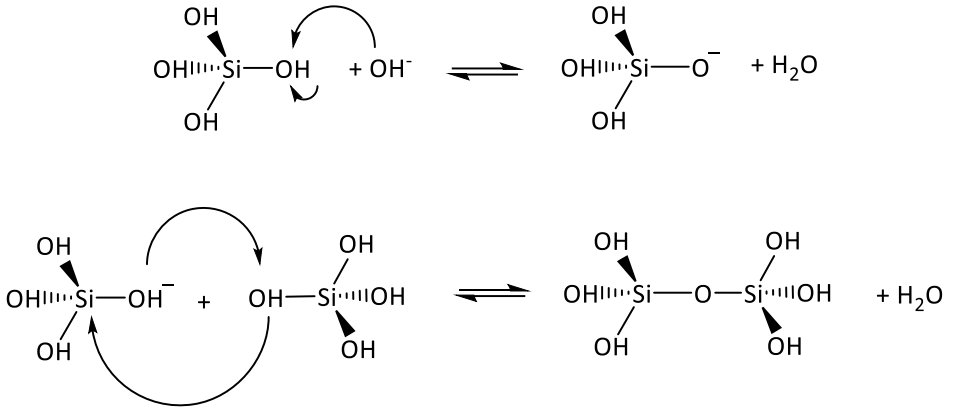

Source: Adapted from [78].

In the second stage, corresponding to polycondensation reactions, a hydroxide ion performs a nucleophilic attack on the hydrogen atom of a silanol group generated during the hydrolysis step. This process leads to the formation of an anionic intermediate, which, in the rapid phase of the mechanism, renders the silicon atom more susceptible to subsequent nucleophilic attacks. Thus, condensation occurs between the oxygen atom of a silanol group and the silicon atom of another silica monomer, resulting in the formation of a siloxane (Si-O-Si) linkage.

Among the starting compounds employed, tetraethyl orthosilicate (TEOS), ammonia, ethanol, and water are particularly noteworthy. The main advantages of this procedure include: (*i*) the formation of homogeneous colloidal suspensions with narrow size distribution and uniform particle morphology; (*ii*) facilitation of the investigation and elucidation of physicochemical and morphological properties; and (*iii*) low cost in the synthesis of nanoparticles[79].

Furthermore, several experimental parameters can be adjusted, directly influencing the final characteristics of the material. For example, the concentration of TEOS and ammonia are closely related to the size and size distribution of the nanoparticles, as they govern the rates of hydrolysis and condensation reactions. Additional factors, such as the synthesis temperature and the agitation rate, can also significantly affect the properties of the resulting product[80].

1.6 LITERATURE REVIEW

For the literature review, an initial survey was conducted on the various synthesis methods reported for the $GdAlO_3$ matrix. **Table 6** compares different methodologies employed for rare-earth ion-doped perovskite matrices and their respective applications.

Table 6. Comparison of different synthesis methods for the perovskite-type $GdAlO_3:RE^{3+}$ matrix.

Synthesis method	Dopant	Advantage	Disadvantage	Heat treatment	Application	Ref.
Hydrothermal	-	Lower calcination temperature, higher crystallinity, and morphological control	Longer heat treatment duration	600 and 700 °C / 180 MPa and 92 h	Displays	[81]
Co-precipitation	-	Uniform materials	High number of steps and heat treatment	1500 °C / 5 h	Radiation detection	[82]
Solid-state reaction	Eu^{2+} and Dy^{3+}	Low environmental impact	Poor morphological control and high energy expenditure	1000 °C / 1 h and 1400 °C / 4 h with N_2 atmosphere	Displays	[83]
Optical floating zone	Tb^{3+}	Morphological control and high growth rate	High energy consumption and high temperatures	1500 °C / 3 h	Scintillator	[84]
Pechini	Eu^{3+} and Tb^{3+}	Wet process with phase formation at milder temperatures	Low morphological control	700, 900, and 1100 °C / 4 h	Scintillator	[65]
Sol-gel	Eu^{3+} and Dy^{3+}	Formation of homogeneous phase experimental simplicity.	High duration in heat treatment and energy expenditure	1000 °C / 10 h	Ceramics	[85]

Source: Prepared by the author.

From this analysis, it was observed that, although several synthesis methods have been reported for the preparation of the $GdAlO_3$ phase, the literature review did not identify studies in which this material was explored for applications in anti-counterfeiting printing technologies. Therefore, the search for studies involving this phase in security-related applications led to investigations employing the combustion method, which is regarded as an efficient alternative for the synthesis of host matrices for DS and UC ions due to its practicality

and environmental advantages. Variations in the dopant ions and synthesis conditions reported in these studies are summarized in **Table 7**.

Table 7. Literature reports on the urea combustion method applied to prepare $GdAlO_3:RE^{3+}$ perovskite-type phosphors and their applications.

Dopant	Fuel	Oxidant	Heat treatment	Application	Ref.
Ce^{3+}	Oxalyl dihydrazide	Metallic nitrates	500 °C / 5 min 900 °C / 3 h	Anti-counterfeiting	[61]
Eu^{3+}	Urea	Metallic nitrates	400 °C / 15 min 900 °C / 3 h	Thermometry and anti-counterfeiting	[62]
Sm^{3+}	Urea	Metallic nitrates	600 °C / 12 min 800, 950, and 1100 °C / 3 h	Solid-state lighting (SSL)	[86]
Tb^{3+}	Urea	Metallic nitrates	600 °C / 12 min 800, 950, and 1100 °C / 3 h	Displays	[87]
Dy^{3+}	Urea	Metallic nitrates	600 °C / 12 min 800, 950, and 1100 °C / 3 h h	WLEDs	[67]
Yb^{3+}	Urea	Metallic nitrates	500 °C / < 3 min 600-900 °C / 2 h	Laser	[88]

Source: Prepared by the author.

In this context, the limited number of literature reports addressing this phase and its application in security-related systems highlights the relevance of further investigation. Therefore, with a view toward the commercial-scale application of luminescent inks in anti-counterfeiting, the urea-assisted combustion method is particularly attractive in the present study due to its low cost and experimental simplicity. Furthermore, to enhance the hydrophilicity of the material and, consequently, its compatibility with the polymeric matrices used in ink formulation, **Table 8** summarizes literature reports on the SiO_2 coating of different inorganic matrices.

Table 8. Summary of literature reports on SiO_2-coated core@shell systems.

Material	Coating method	Shell thickness	Application	Ref
$Gd_2SiO_5:Tb^{3+}@SiO_2$	Stöber	45 nm	Photodynamic therapy	[89]
$NaYF_4:Er,Yb@SiO_2$	Stöber	50 nm	Anti-counterfeiting printing	[90]
$Ca\text{-}Eu:Y_2O_3@SiO_2$	Stöber adapted	25 nm	Optoelectronic	[91]
$Na_3GaF_6:Tm^{3+},Yb^{3+}@SiO_2$	Stöber	3.2 nm	Cryptography in anti-counterfeiting	[92]

Source: Prepared by the author.

Notably, during this survey, no literature reports were found on the use of SiO_2-coated $GdAlO_3$ matrices as a luminescent ink for anti-counterfeiting applications, underscoring

the novelty of this research. Finally, to explore different ink formulations and their potential use in security technologies, a complementary literature search was conducted on materials compatible with dispersion in polymeric matrices, as summarized in **Table 9.**

Table 9. Literature review of luminescent inks based on different polymer matrices and substrates.

Material	Polymeric matrix	Application technique	Excitation / nm	Substrate	Ref.
SiO_2@$LaPO_4$: $Er_{0.1}Eu_x$@SiO_2	H_2O:EtOH:Glycerol	Luminescent patterns	254, 365, and 980	Paper	[93]
$LaGeSbO_6$:Eu^{3+}	PVA	Cryptography	275	Glass, aluminum foil, and black cardboard	[94]
Y_2O_3:Eu^{3+}	PVA	Luminescent patterns	250. 365, and 395	Black paper	[95]
$CaYGaO_4$:Eu^{3+}	Commercial ink	Luminescent patterns	393	Glass, plastic, and kraft paper	[96]
Ca_2GaO_4:Eu^{3+}	PVA	Luminescent patterns	395	Black paper, glass, paper, and barcode	[97]
$BaLaGaO_4$:Sm^{3+}	PVA	Luminescent patterns	365	Black paper, glass, kraft paper, and paper labels	[98]
C_2GaTaO_6:Sm^{3+}	PVA	Luminescent patterns	365	Kraft paper, ceramics and glass	[99]

Source: Prepared by the author.

Therefore, the survey indicates that polyvinyl alcohol (PVA) and glycerol, when employed as polymeric matrices in ink formulations, promote adequate dispersion of phosphor/core@shell systems within the polymer medium, while also offering advantages such as low cost, non-toxicity, and environmental compatibility. Furthermore, a scarcity of studies describing the synthesis of luminescent inks exhibiting upconversion properties was identified. Finally, no literature reports were found exploring the phase of interest in ink formulations applied to techniques such as screen printing and calligraphy.

1.7 GROUP TIMELINE

Among the research lines developed at the Laboratory of Luminescence in Materials and Sensors (LLuMeS), located at the Faculty of Science and Technology of UNESP in Presidente Prudente (SP) and coordinated by Professors Ana Maria Pires and Sergio Antonio Marques de Lima, the synthesis of inorganic matrices for the production of solid luminescent materials exhibiting downshifting (DS) and/or upconversion (UC) properties stand out. These phosphors find applications in SSL, including LEDs and OLEDs, as well as in cell imaging, and

solar cells. Within the scope of the present work, a new application is introduced within the group, namely the development of luminescent materials aimed at anti-counterfeiting systems.

Within the group, different host matrices and synthetic routes have been investigated, with particular emphasis on the modified Pechini method. Shinohara (2016)[100] evaluated the influence of the polymerizing agent, ethylene glycol versus sorbitol, on the synthesis of Y_2O_3:Eu^{3+} and demonstrated, using chemometric tools, that the use of sorbitol promotes higher emission intensity, while also offering advantages such as low cost and reduced toxicity.

Subsequently, Costa *et al.* (2020)[101] developed Y_2O_3:RE^{3+}@SiO_2-[RE^{3+}(β-diketonated)$_3$] core@shell hybrid materials for bioimaging applications, establishing key parameters for SiO_2 coating via the modified Stöber method. In addition, Oliveira *et. al* (2021, 2022)[102,103] investigated the Y_2O_3:Eu^{3+},Er^{3+},Yb^{3+} systems exhibiting DS and UC properties, as well as $BaAl_2O_4$:Eu^{3+} (DS) system, comparing different synthetic routes, elucidating energy transfer mechanisms, and optimizing both structural and luminescent properties.

Other host matrices have also been investigated within the group, including Ba_2SiO_4:Eu^{3+}/Tb^{3+}, Sr_2SiO_4:Eu^{2+} systems reported by Bispo-Jr, A.G. *et al.* (2017, 2019, and 2020)[104,105,106], as well as $MgAl_2O_4$:Eu^{3+} studied by Mesti, M.E.M. (2024)[107]. These materials were explored for solid-state lighting (SSL) applications, such as circadian cycle regulation, and luminescent thermometry. Comprehensive structural, morphological, and spectroscopic analyses enabled an understanding of the effects of dopant concentration and co-doping on site occupancy and emission efficiency.

In his master's and doctoral thesis, Garcia, A.B.S. (2019, 2024)[108,109] investigated inorganic-organic hybrid $LaAlO_3$-based multishell materials exhibiting DS[110] and UC[111] properties, synthesized using the Pechini and Stöber methods, for application in light-conversion devices and luminescent thermometry. In the master's study, focused on DS emission, the formation of the target phase was confirmed after rare-earth doping, SiO_2 coating, and subsequent aminofunctionalization. In the doctoral work, the $GdAlO_3$ phase was explored as a shell in $LaAlO_3$:Er^{3+},Yb^{3+} systems, demonstrating promising performance in UC processes.

It is noteworthy that the introduction of $GdAlO_3$ as a shell in hybrid structures constituted the key motivation for the present work, stimulating interest in exploring this

phase as a host matrix for optically active ions excitable in the UV and IR regions. Accordingly, this study builds directly upon that structural strategy, advancing to the synthesis of the $GdAlO_3$ as the primary host matrix, followed by SiO_2 coating to obtain core@shell-type systems. Moreover, the availability of well-established experimental conditions for this phase in the literature, together with the wide range of possible dopant ions and the absence of reports on the use of $GdAlO_3$-based materials as luminescent inks for anti-counterfeiting applications, rendered this material particularly suitable for the proposed investigation.

Finally, during my undergraduate research, I investigated the orthorhombic SrY_2O_4 matrix doped with $Ce^{3+/4+}$ and/or Eu^{3+}, aiming to evaluate the effect of varying $Ce^{3+/4+}$ concentrations as sensitizing ion, based on the work developed by Saraiva, L.F. *et al.* (2023)[112]. For the Eu^{3+}-doped phosphors, luminescent thermometry studies were conducted using both ratiometric and multiparametric approaches. In addition to these dopants, Tb^{3+} ions were also incorporated into the SrY_2O_4 matrix to assess phase stabilization and explore potential applications in green-emitting luminescent films for solid-state lighting.

Figure 12 illustrates the timeline of research activities on inorganic matrices developed by the research group, which ultimately led to the present master's dissertation.

Figure 12. Illustrative representation of research activities carried out within the group that contributed to the formulation and development of the master's thesis project.

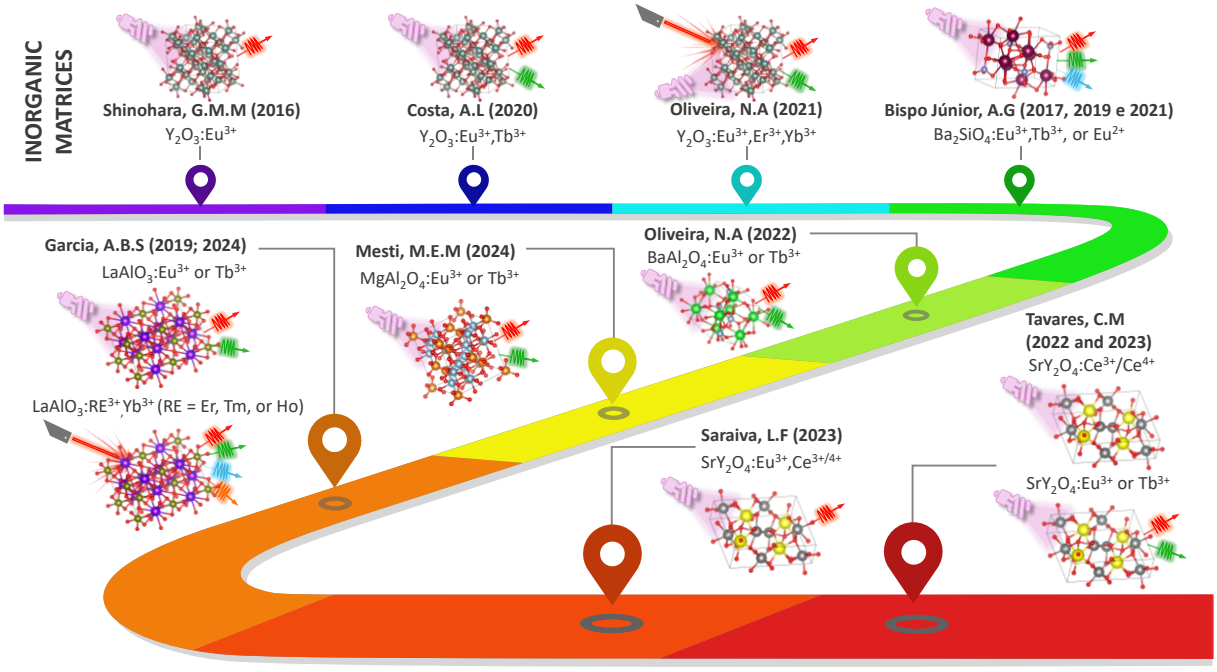

Source: Prepared by the author.

To contextualize the work presented below, the synthesis stages and a substantial portion of the structural and molecular characterization associated with this master's dissertation were carried out at institutions in Brazil. In contrast, the fabrication of the luminescent inks was performed at the Luminescence Laboratory of the *Universidad de Chile*, Ñuñoa campus, in Santiago. Furthermore, part of the printing-patterns applications was developed in collaboration with the *Universidad Austral de Chile* (UACh), in Valdivia, during the internship.

5 CONCLUSION

In structural terms, X-ray diffraction data for all $GdAlO_3:Ln^{3+}$ (Eu or Er/Yb) phosphors confirmed the successful formation of the orthorhombic perovskite phase (space group *Pbnm*), as well as the stability of the phase before and after doping with Ln^{3+} ions, as evidenced by the evaluation of tolerance factors. These data results complemented by Rietveld structural refinement, further confirming the effectiveness of the urea combustion method. Additionally, lattice parameters were extracted, indicating effective substitution of the dopant ions at C_s symmetry sites of the octacoordinated Gd^{3+} ions, in agreement with literature reports. The average crystallite size data reinforces the crystallinity of the materials.

IR spectra complement the structural analysis by revealing vibrational modes associated with the characteristic stretching and bending of metal-oxygen bonds. In the XRD measurements of the SiO_2-containing systems, no typical amorphous halo attributable to silica was observed in the diffraction patterns. This behavior is consistent with the presence of a thin SiO_2 coating on the particles, which may be below the detection limit of X-ray diffraction, and was further investigated by TEM analysis. However, complementary IR spectroscopy confirmed the presence of SiO_2 through the identification of antisymmetric stretching bands around 1100 cm^{-1}, characteristic of Si–O–Si vibrations.

From TEM images of the GAP and GAP5Eu samples, as well as their respective SiO_2 modified counterparts, and supported by EDS analysis of GAP5Eu, it was possible to conclude that a considerable degree of particle agglomeration occurs even prior to surface modification with SiO_2. This behavior is attributed to the coalescence and mass transfer process during the calcination step, which are typical of materials synthesized via the urea combustion method. However, a high degree of crystallinity was observed, as evidenced by the presence of lattice fringes and the assignment of the (101) crystallographic plane to the GAP5Eu sample.

Regarding the spectroscopic characterization of the phosphors, UV-Vis diffuse reflectance (DR) measurements for the Eu^{3+}-doped series complement the photoluminescence (PL) data, enabling the identification of the main absorption regions across all concentrations. The optical band gap was found to vary from 3.24 eV to 3.32 eV with increasing Eu^{3+} concentration.

PL measurements revealed similar spectral profiles for samples modified or not with SiO_2, even at low temperature, in the case of Eu^{3+} as the dopant, with a high degree of

color purity in the red-orange region of the spectrum. Furthermore, it was possible to confirm dopant incorporation into at least one C_s symmetry site based on the observed behavior of the $^7F_0 \rightarrow {}^5D_0$, $^7F_0 \rightarrow {}^5D_1$, and $^7F_0 \rightarrow {}^5D_2$ transitions. When excited at 395 nm (*f-f* transitions), the spectral profile was preserved.

Kinetic lifetime measurements revealed biexponential behavior for the downshifting systems, with average lifetimes ranging from 1.18-2.51 ms. A higher Φ_{Eu}^{L} value of 66.9% was observed for the GAP5Eu sample, while Φ_{Eu}^{Eu} reached 50.1% for GAP1Eu under excitation at 263 nm. In general, modification with SiO_2 led to luminescence quenching, evidenced by the decrease in quantum yield.

The spectral profile of the UC systems remained stable after modification with SiO_2 and upon lowering the temperature, exhibiting a high degree of color purity in the green region. Measurements performed with varying laser power (25–400 mW) revealed a two-photon process, attributed to the energy transfer upconversion (ETU) mechanism. Kinetic measurements of the phosphors showed monoexponential decay behavior, with lifetimes decreasing from 0.40 to 0.040 ms as a function of increasing sensitizer (Yb^{3+}) concentration.

Zeta potential measurements for the luminescent inks confirm the experimental observed sedimentation behavior, based on the relationship between the isoelectric point and the pH of the medium. Histograms of the average particle diameter obtained by DLS reflect the degree of agglomeration and are further supported by the *PdI* values for both multifunctional inks. IR analysis of the inks revealed the main stretching and bending vibrations associated with each polymeric matrix used.

The emission spectra collected from the inks formulated with both polymer matrices preserved the spectral profile, exhibiting the main DS and UC transitions and confirming the dual multifunctional character of the materials. The kinetic behavior remained similar to that of the respective precursor phosphors, with a decrease in lifetime attributed to increased non-radiative rates due to the presence of quenchers (–OH) in the chemical structure of the polymers.

Finally, the applied printing techniques confirm the promising applicability of the inks on different substrates. For calligraphy, the PVA-based ink proved suitable for rapid tests and for assessing ink adhesion to the substrate. Stamping was effective on black paper and banknotes, providing transparency under ambient light. Screen printing did not exhibit visible emission under the selected excitation wavelength, likely due to the mesh size employed. In

contrast, the spray coating technique proved effective on brown paper and enabled good dispersion of the UC phosphor within the pattern.

Therefore, the synthesis of precursor phosphors (with or without SiO_2-modified surfaces), the formulation of dual-emission multifunctional luminescent inks, and their application across different printing technologies demonstrated significant advances in anti-counterfeiting, enabling their use in security systems requiring specialized authentication.

REFERENCES

[1] HUANG, S.; MUKUNDAN, A.; TSAO, Y.; KIM, Y.; LIN, F.; WANG, H. Recent Advances in Counterfeit Art, Document, Photo, Hologram, and Currency Detection Using Hyperspectral Imaging. **Sensors**, v. 22, p. 7308, 2022. DOI: 10.3390/s22197308. Available in: https://www.mdpi.com/1424-8220/22/19/7308.

[2] QUERCIOLI, E.; SMITH, L. The Economics of Counterfeiting. **Econometrica**, v. 83, p. 1211-1236, 2015. DOI: 10.3982/ECTA10975. Available in: https://onlinelibrary.wiley.com/doi/abs/10.3982.

[3] POLAK, A.; KELMAN, T.; MURRAY, P.; MARSHALL, S.; STOTHARD, D. J. M.; EASTAUGH, N.; EASTAUGH, F. Hyperspectral imaging combined with data classification techniques as an aid for artwork authentication. **Journal of Cultural Heritage**, v. 26, p. 1-11, 2017. DOI: 10.1016/j.culher.2017.01.013. Available in: https://www.sciencedirect.com/science/article/pii/S1296207417301218.

[4] SILVA, C. S.; PIMENTAL, M. F.; HONORATO, R. S.; PASQUINI, C.; PRATS-MONTALBÁN, J. M.; FERRER, A. Near infrared hyperspectral imaging for forensic analysis of document forgery. **Analyst**, v. 139, p. 5176-5184, 2014. DOI: 10.1039/C4AN00961D. Available in: https://pubs.rsc.org/en/content/articlelanding/2014/an/c4an00961d.

[5] NGUYEN, T. P.; DANG, H. P.; NGUYEN, L. G.; LE, C. D. Synthesis of ZnO nanoparticles-based fluorescent ink for information encryption and security applications. **Optical Materials**, v. 157, p. 116296, 2024. DOI: 10.1016/j.optmat.2024.116296. Available in: https://www.sciencedirect.com/science/article/pii/S0925346724014794.

[6] KIM, H.; BEACK, S.; HAN, S.; SHIN, M.; LEE, T.; PARK, Y.; KIM, K. S.; YETISEN, A. K.; YUN, S. H.; KWON, W.; HAHN, S. K. Multifunctional Photonic Nanomaterials for Diagnostic, Therapeutic, and Theranostic Applications. **Advanced Materials**, v. 30, p. 1701460, 2018. DOI: 10.1002/adma.201701460. Available in: https://advanced.onlinelibrary.wiley.com/doi/full/10.1002/adma.201701460.

[7] PHILLIPS, J. M.; COLTRIN, M. E.; CRAWFORD, M. H.; FISCHER, A. J.; KRAMES, M. R.; MUELLER-MACH, R.; MUELLER, G.O.; OHNO, Y.; ROHWER, L.E.S.; SIMMONS, J.A.; TSAO, J. Y. Research challenges to ultra-efficient inorganic solid-state lighting. **Laser & Photonics Reviews**, v. 1, p. 307-333, 2007. DOI: 10.1002/lpor.200710019. Available in: https://onlinelibrary.wiley.com/doi/abs/10.1002/lpor.200710019.

[8] XU, C.; HUANG, C.; YANG, D.; LUO, L.; HUANG, S. Photo-Luminescent Photonic Crystals for Anti-Counterfeiting. **ACS Omega**, v.7, p. 7320-7326, 2022. DOI: 10.1021/acsomega.1c07150. Available in: https://pubs.acs.org/doi/full/10.1021/acsomega.1c07150.

[9] NAIR, R. V.; WANG, F.; YANG, X.; JAGADISH, C. Photonic materials: from fundamentals to applications. **The European Physical Journal Special Topics**, v. 231, p. 583-587, 2022. DOI:

10.1140/epjs/s11734-022-00541-6. Available in: https://link.springer.com/article/10.1140/epjs/s11734-022-00541-6.

[10] LIANG, X.; ZHANG, F.; GONG, H.; WEI, R.; GUO, H.; HU, F. Dual-mode optical thermometry and multilevel anti-counterfeiting based on Er3+/Eu3+ doped Ba5Gd8Zn4O21 phosphors. **Journal of Luminescence***,* v. 269, p. 120483, 2024. DOI: 10.1016/j.jlumin.2024.120483. Available in: https://www.sciencedirect.com/science/article/pii/S0022231324000474.

[11] ZHOU, X.; NING, L.; QIAO, J.; ZHAO, Y.; XIONG, P.; XIA, Z. Interplay of defect levels and rare-earth emission centers in multimode luminescent phosphors. **Nature Communications**, v. 13, p. 7589, 2022. DOI: 10.1038/s41467-022-35366-3. Available in: https://www.nature.com/articles/s41467-022-35366-3.

[12] NADORT, A.; ZHAO, J.; GOLDYS, E. M. Lanthanide upconversion luminescence at the nanoscale: fundamentals and optical properties. **Nanoscale**, v. 8, p. 13099-13130, 2016. DOI: 10.1039/C5NR08477F. Available in: https://pubs.rsc.org/en/content/articlehtml/2016/nr/c5nr08477f.

[13] SOUSA FILHO, P. C.; LIMA, J. F.; SERRA, O. A. From Lighting to Photoprotection: Fundamentals and Applications of Rare-earth Materials. **Journal of the Brazilian Chemical Society**, v. 26, 2471-2495, 2015. DOI: 10.5935/0103-5053.20150328. Available in: https://www.scielo.br/j/jbchs/a/Zfm7qbKj9BRNZgLFCgkCpjg/?lang=en.

[14] GUPTA, I.; SINGH, S.; BHAGWAN, S.; SINGH, D. Rare-earth (RE) doped phosphors and their emerging applications: A review. **Ceramics International**, v. 47, p. 19282-19303, 2021. DOI: 10.1016/j.ceramint.2021.03.308. Available in: https://www.sciencedirect.com/science/article/pii/S0272884221010154.

[15] SPARKS, J. S.; SCHELLY, R. C.; SMITH, W. L.; DAVIS, M. P.; TCHERNOV, D.; PIERIBONE, V. A.; GRUBER, D. F. The Covert World of Fish Biofluorescence: A Phylogenetically Widespread and Phenotypically Variable Phenomenon. **PLoS ONE**, v. 8, p. e83259, 2013. DOI: 10.1371/journal.pone.0083259. Available in: https://journals.plos.org/plosone/article?id=10.1371/journal.pone.0083259.

[16] KÖHLER, A.; WILSON, J. S.; FRIEND, R. H. Fluorescence and Phosphorescence in Organic Materials. **Advanced Engineering Materials**, v. 4, p. 453-459, 2002. DOI: 10.1002/1527-2648(20020717)4:7. Available in: https://advanced.onlinelibrary.wiley.com/doi/abs/10.1002/1527-2648(20020717)4:7.

[17] SMET, P. F.; MOREELS, I.; HENS, Z.; POELMAN, D. Luminescence in Sulfides: A Rich History and a Bright Future. **Materials**¸ v. 3, p. 2834-2883, 2010. DOI: 10.3390/ma3042834. Available in: https://www.mdpi.com/1996-1944/3/4/2834.

[18] BLASSE, G.; GRABMAIER, B. C. A general introduction to luminescent materials. *In:* **Luminescent materials.** Berlin, Heidelberg: Springer Berlin Heidelberg, 1994. p. 1-9.

[19] THOMPSON, S. M.; SAHIN, C.; YANG, S.; FLATTÉ, M. E.; MURRAY, C. B.; BASSETT, L. C.; KAGAN, C. R. Red Emission from Copper-Vacancy Color Centers in Zinc Sulfide Colloidal

Nanocrystals. **ACS Nano**, v. 17, p. 5963-5973, 2023. DOI: doi.org/10.1021/acsnano.3c00191. Available in: https://pubs.acs.org/doi/full/10.1021/acsnano.3c00191.

[20] NETTOUR, R.; KABIR, A.; ERDOGMUS, A.; KUTLU, O. D.; SCHMERBER, G. Structural, optical and luminescence characterization of Co-doped ZnO thin films. **Micro and Nanostrucures**, v. 207, p. 208271, 2025. DOI: doi.org/10.1016/j.micrna.2025.208271. Available in: https://www.sciencedirect.com/science/article/pii/S2773012325002006.

[21] HUAN, V. D.; QUANG, N. V.; TU, N.; HUY, P. T. Dual green and red emitting Mn-doped $MgAl_2O_4$ phosphors for WLED and plant growth LED applications. **Journal of Alloys and Compounds**, v. 1027, p. 180621, 2025. DOI: doi.org/10.1016/j.jallcom.2025.180621. Available in: https://www.sciencedirect.com/science/article/pii/S0925838825021826.

[22] WANG, H.; BATENTSCHUK, M.; OSVET, A.; PINNA, L.; BRABEC, C. J. Rare-Earth Ion Doped Up-Conversion Materials for Photovoltaic Applications.
Advanced Materials, v. 23, p. 2675-2680, 2011. DOI: 10.1002/adma.201100511. Available in: https://advanced.onlinelibrary.wiley.com/doi/full/10.1002/adma.201100511.

[23] BRITO, H. F.; MALTA, O. M. L.; FELINTO, M. C. F. C.; TEOTONIO, E. E. de S. Luminescence phenomena involving metal enolates. **PATAI'S Chemistry of Functional Groups**, 2010. DOI: 10.1002/9780470682531.pat0419. Available in: https://onlinelibrary.wiley.com/doi/abs/10.1002/9780470682531.pat0419.

[24] DIEKE, G. H.; SATTEN, R. A. Spectra and Energy Levels of Rare-earth Ions in Crystals. **American Journal of Physics**, v. 38, p. 399-400, 1970. DOI: 10.1119/1.1976350. Available in: https://pubs.aip.org/aapt/ajp/article-abstract/38/3/399/1040957.

[25] CARNALL, W. T.; FIELDS, P. R.; RAJNAK, K. Electronic Energy Levels in the Trivalent Lanthanide Aquo Ions. I. Pr^{3+}, Nd^{3+}, Pm^{3+}, Sm^{3+}, Dy^{3+}, Ho^{3+}, Er^{3+}, and Tm^{3+}. **The Journal of Chemical Physics**, v. 49, p. 4424-4442, 1968. DOI: 10.1063/1.1669893. Available in: https://pubs.aip.org/aip/jcp/article-abstract/49/10/4424/211521.

[26] SIGOLI, F.A.; BISPO-JR, A. G.; DE SOUSA FILHO, P.C. **Lantanídeos: química, luminescência e aplicações**. Campinas: Editora Átomo, 2022.

[27] HUH, Y.; CHO, Y.; DO, Y. R. The Optical Properties of $(Y_{1-x}Gd_x)_{3-z}(Al_{1-y}Ga_y)_5O_{12}:Ce_z$ Phosphors for White LED. **Bulletin of the Korean Chemical Society**, v. 23, p. 1435-1438, 2002. DOI: 10.5012/bkcs.2002.23.10.1435. Available in: https://citeseerx.ist.psu.edu/document/10.5012/bkcs.2002.23.10.1435.

[28] TALLANT, D.R.; SEAGER, C.H.; SIMPSON, R.L. Energy transfer and relaxation in europium-activated Y_2O_3 after excitation by ultraviolet photons. **Journal of Applied Physics**, v. 91, p. 4053-4064.

[29] DEXTER, D. L. Possibility of Luminescent Quantum Yields Greater than Unity. **Physical Review**, v. 108, p. 630, 1957. DOI: 10.1103/PhysRev.108.630. Available in: https://journals.aps.org/pr/abstract/10.1103/PhysRev.108.630.

[30] JOSHI, A.; RASSKAZOV, I. L. Plasmon-enhanced downshifting and downconversion: Fundamentals and applications in photovoltaics. **Reviews in Physics**, v. 12, p. 100096, 2024. DOI: 10.1016/j.revip.2024.100096. Available in: https://www.sciencedirect.com/science/article/pii/S2405428324000066.

[31] DEL-CASTILLO, J.; YANES, A. C.; CANTÓN-JARA, M. Efficient down-shifting and up-conversion emission dual-mode in RE^{3+}-doped $NaTbF_4$-based nano-glass ceramics. **Journal of Materials Chemistry C**, v. 11, p. 7662, 2023. DOI: 10.1039/D3TC00816A. Available in: https://pubs.rsc.org/en/content/articlehtml/2023/tc/d3tc00816a.

[32] AUZEL, F. ompteur quantique par transfert d'energie entre deux ions de terres rares dans un tungstate mixte et dans un verre. **Comptes Rendus de l'Académie des Sciences Paris**, 262, p. 1016-1019, 1966. Available in: https://cir.nii.ac.jp/crid/1573950399692310784.

[33] WANG, S.; ZHU, J.; HE, Y.; LI, Z.; LIN, J.; LIAO, S.; HUANG, F.; HUANG, P.; ZHENG, Y.; LI, X.; CHEN, D. Invisible NIR Spectral Imaging and Laser-Induced Thermal Imaging of Na(Nd/Y)F_4@glass with Opposite Effect for Optical Security. **Laser & Photonics Reviews**, v. 16, p. 2200039, 2022. DOI: 10.1002/lpor.202200039. Available in: https://onlinelibrary.wiley.com/doi/full/10.1002/lpor.202200039.

[34] ZHENG, K.; LOH, K. Y.; WANG, Y.; CHEN, Q.; FAN, J.; JUNG, T.; NAM, S. H.; SUH, Y. D.; LIU, X. Recent advances in upconversion nanocrystals: Expanding the kaleidoscopic toolbox for emerging applications. **Nano Today**, v. 29, p. 100797, 2019. DOI: 10.1016/j.nantod.2019.100797. Available in: https://www.sciencedirect.com/science/article/pii/S1748013219302555.

[35] JIA, Y.; SHI, Z.; WANG, J.; LI, X.; ZHAO, Z. Fluorescence properties of LaOF: Er, Eu phosphors and their application in fluorescence anti-counterfeiting. **Journal of Luminescence**, v. 253, p. 119489, 2023. DOI: 10.1016/j.jlumin.2022.119489. Available in: https://www.sciencedirect.com/science/article/pii/S0022231322007645.

[36] BINNEMANS, K. Interpretation of europium(III) spectra. **Coordination Chemistry Reviews**, v. 295, p. 1-45, 2015. DOI: 10.1016/j.ccr.2015.02.015. Available in: https://www.sciencedirect.com/science/article/pii/S001085451500065.

[37] MAHAKHODE, J.G.; NANDE, A.; DHOBLE, S.J. A review: X-ray excited luminescence of gadolinium based optoelectronic phosphors. **Luminescence**, v. 36, p. 1344-1353, 2021. DOI: 10.1002/bio.4081Digital. Available in: https://analyticalsciencejournals.onlinelibrary.wiley.com/doi/full/10.1002/bio.4081.

[38] VETRONE, F.; BOYER, J. C.; CAPOBIANCO, J. A.; SPEGHINI, A.; BETINELLI, M. Effect of Yb^{3+} Codoping on the Upconversion Emission in Nanocrystalline Y_2O_3:Er^{3+}. **The Journal of Physical Chemistry B**, v. 107, p. 1107-1112, 2003. DOI: 10.1021/jp0218692. Available in: https://pubs.acs.org/doi/full/10.1021/jp0218692.

[39] BISPO-JR, A.G. Multifunctional lanthanide(III) single-molecule magnets displaying luminescence thermometry: Progress, challenges, and future directions. **Coordination**

Chemistry Reviews, v. 537, p. 216685, 2025. DOI: 10.1016/j.ccr.2025.216685. Available in: https://www.sciencedirect.com/science/article/pii/S0010854525002553.

[40] BARRERA, J. F.; MIRA, A.; TORROBA, R. Optical encryption and QR codes: Secure and noise-free information retrieval. **Optics Express**, v. 21, p. 5373-5378, 2013. DOI: 10.1364/OE.21.005373. Available in: https://opg.optica.org/oe/fulltext.cfm?uri=oe-21-5-5373&id=249515.

[41] TUYLS, P.; BATINA, L. RFID-Tags for Anti-counterfeiting. **Topics in Cryptology – CT – RSA**, v. 3860, p. 115-131, 2006. DOI: 10.1007/11605805_8. Available in: https://link.springer.com/chapter/10.1007/11605805.

[42] GOH, X. M.; ZHENG, Y.; TAN, S. J.; ZHANG, L.; KUMAR, K.; QIU, C.; YANG, J. K. W. Three-dimensional plasmonic stereoscopic prints in full colour. **Nature communications**, v. 5, p. 5361, 2014. DOI: 10.1038/ncomms6361. Available in: https://www.nature.com/articles/ncomms6361.

[43] MCGREW, S. P. Hologram Counterfeiting: Problems and Solutions. **Optical and anticounterfeiting systems**, v. 1210, p. 66-76, 1990. DOI: 10.1117/12.17915. Available in: https://www.spiedigitallibrary.org/conference-proceedings-of-spie/1210/1/Hologram-counterfeiting-problems-and-solutions/10.1117/12.17915.short.

[44] PUSHPENDRA; NAIDU, B. S. Luminescent nanomaterials based covert tags for anti-counterfeiting applications: A review. **Advances in Colloid and Interface Science**, v. 341, p. 103480, 2025. DOI: 10.1016/j.cis.2025.103480. Available in: https://www.sciencedirect.com/science/article/pii/S0001868625000910#bb0265.

[45] KUMAR, P.; DWIVED, J.; GUPTA, B. K. Highly luminescent dual mode rare-earth nanorod assisted multi-stage excitable security ink for anti-counterfeiting applications. **Journal of Materials Chemistry C**, v. 2, p. 10468-10475, 2014. DOI: 10.1039/C4TC02065K. Available in: https://pubs.rsc.org/en/content/articlelanding/2014/tc/c4tc02065k/unauth.

[46] ABDOLLAHI, A.; ROGHANI-MAMAQANI, H.; RAZAVI, B.; SALAMI-KALAJAHI, M. Photoluminescent and Chromic Nanomaterials for Anticounterfeiting Technologies: Recent Advances and Future Challenges. **ACS Nano**, v. 14, p. 14417-14492, 2020. DOI: 10.1021/acsnano.0c07289. Available in: https://pubs.acs.org/doi/pdf/10.1021/acsnano.0c07289.

[47] LUŇÁKOVÁ, M.; DORAZIL, J.; JONÁK, M.; JEŽEK, S.; URGET, R. Pen Ink Library: An interactive database of writing instruments based on Vis-NIR reflection spectra and optical properties of inks. **Forensic Science International**, v. 373, p. 112508, 2025. DOI: 10.1016/j.forsciint.2025.112508. Available in: https://www.sciencedirect.com/science/article/pii/S037907382500146X.

[48] ABOU-MELHA, K. Preparation of photoluminescent nanocomposite ink toward dual-mode secure anti-counterfeiting stamps. **Arabian Journal of Chemistry**, v. 15, p. 103604, 2022. DOI: 10.1016/j.arabjc.2021.103604. Available in: https://www.sciencedirect.com/science/article/pii/S1878535221006195.

[49] S ARMA, S. . Exploring the potential of aLa_2ZnO_5 doped with individual rare-earth ions (Ce^{3+}, Er^{3+}, Eu^{3+}) for w-LEDs, latent fingerprints, and anti-counterfeiting applications. **Journal of Luminescence**, v. 278, p. 120994, 2025. DOI: 10.1016/j.jlumin.2024.120994. Available in: https://www.sciencedirect.com/science/article/pii/S0022231324005581.

[50] AMIN, S.; PANCHAL, H. A review on thermal spray coating processes. **International Journal of Current Trends in Engineering & Research**, v. 2, n. 4, p. 556-563, 2016. Available in: https://poudrafshan.ir/wp-content/uploads/2019/05/A-Review-on-Thermal-Spray coating-Processes-1.pdf.

[51] SAJWAN, R. K.; TIWARI, S.; HARSHIT, T.; SINGH, A. K. Recent progress in multicolor tuning of rare-earth-doped gadolinium aluminate phosphors $GdAlO_3$. **Optical and Quantum Electronics**, v. 49, p. 343-377, 2017. DOI: 10.1007/s11082-017-1158-5. Available in: https://link.springer.com/article/10.1007/s11082-017-1158-5.

[52] AKATSUKA, M.; OKADA G.; NAKAUCHI D.; KATO T.; KAWAGUCHI N.; YANAGIDA T. Scintillation properties of $GdAlO_3$ crystals doped with different concentrations of Tm. **Journal of Luminescence**, v. 228, p. 117610, 2020. DOI: 10.1016/j.jlumin.2020.117610. Available in: https://www.sciencedirect.com/science/article/pii/S0022231320307547.

[53] KOURDACI, A. E.; BOURACHID I.; BOUAFIA H.; MECHERI K.; ABIDRI K.; RACHED D. First-principles calculations to examine structural, magnetic, mechanical, electronic and optical properties of wide Band gap semiconductor Gadolinium Aluminum Oxide perovskite $GdAlO_3$. **Computational Condensed Matter**, v. 38, p. e00889, 2024. DOI: 10.1016/j.cocom.2024.e00889. Available in: https://www.sciencedirect.com/science/article/pii/S235221432400011X.

[54] ALSOBHI, B. O. First-principles calculations to investigate structural, electronic, magnetic, optical, mechanical and thermoelectric properties of rare-earth aluminate perovskite $XAlO_3$ (X = Ce, Nd, Gd) compounds. **Materials Chemistry and Physics**, v. 301, p. 127691, 2023. DOI: 10.1016/j.matchemphys.2023.127691. Available in: https://www.sciencedirect.com/science/article/pii/S0254058423003991.

[55] CHAUDHURY, S.; PARIDA, S. C.; PILLAI K. T.; SINGH MUDHER K. D. High-temperature X-ray diffraction and specific heat studies on $GdAlO_3$, $Gd_3Al_5O_{12}$ and $Gd_4Al_2O_9$. **Journal of Solid State Chemistry**, v. 180, p. 2393-2399, 2007. DOI: 10.1016/j.jssc.2007.06.003. Available in: https://www.sciencedirect.com/science/article/pii/S0022459607002265.

[56] GUPTA, I.; SINGH D.; SINGH S.; KUMAR P.; BHAGWAN S.; KUMAR V. Study of structural and spectroscopic characteristics of novel color tunable yellowish-white Dy^{3+} doped $Gd_4Al_2O_9$ nanophosphors for NUV-based WLEDs. **Journal of Molecular Structure**, v. 1272, p. 134199, 2023. DOI: 10.1016/j.molstruc.2022.134199.
Available in: https://www.researchgate.net/publication/363776195.

[57] SMIRNOVA, S. A.; KAZAKOVA, L. I; FYODOROV, A. A.; KORZHIK, M. V. Fast and heavy $GdAlO_3$:Ce scintillators. **Journal of Luminescence**, v. 60&61, p. 960-962, 1994. DOI:

10.1016/0022-2313(94)90320-4. Available in: https://www.sciencedirect.com/science/article/pii/0022231394903204.

[58] SHILPA C. J.; NAGABHUSHANA H. Structural and photoluminescence properties of doped $GdAlO_3$ nanophosphors: Applications towards display devices. **Materials Today: Proceedings**, v. 5, p. 21111-21118, 2018. DOI: 10.1016/j.matpr.2018.06.507. Available in: https://www.sciencedirect.com/science/article/pii/S2214785318316407.

[59] RICHARD, D.; MOCCIARO, A.; ANAYA, R. J.; CONCONI, M. S.; RENDTORFF, N. M. $Al_2O_3/GdAlO_3$ reaction sintered composites produced from milled powders: Microstructure, neutron-capture cross section, and mechanical properties. **Ceramics Internation**, v. 49, p. 31839-31845, 2023. DOI: 10.1016/j.ceramint.2023.07.143. Available in: https://www.sciencedirect.com/science/article/pii/S0272884223020710.

[60] FABIÁN, M.; ARIAS-SERRANO, B. I.; BRIANCIN, J.; YAREMCHENKO, A. Mechanosynthesis and electrical conductivity of undoped and calcium-substituted $GdAlO_3$ perovskites. **Journal of Alloys and Compounds**, v. 965, p. 171374, 2023. DOI: 10.1016/j.jallcom.2023.171374. Available in: https://www.sciencedirect.com/science/article/pii/S0925838823026774.

[61] SHILPA, C. J.; *BASAVARAJ*, R. B.; DARSHAN, G. P.; PREMKUMAR, H. B.; SHARMA, S. C.; NAGABHUSHANA, H. New insights into the rapid deposition and visualization of latent fingerprints: Cyan light emitting $GdAlO_3:Ce^{3+}$ nano fluorescent probe. **Journal of Photochemistry & Photobiology A: Chemistry**, v. 376, p. 288-304, 2019. DOI: 10.1016/j.jphotochem.2019.02.027. Available in: https://www.sciencedirect.com/science/article/pii/S1010603018315995.

[62] NAVYA, N.; RADHA KRUSHNA, B. R.; SHARMA, S. C.; SRINIVASAN, A. R.; GEORGE, A.; MOHAPATRA, S. S.; KRITHIKA, C.; BHANU, A.; MANJUNATHA, K.; WU, S. Y.; NAGABHUSHANA, H. *In-situ* embedding of carbon dots in perovskite $GdAlO_3:Eu^{3+}/Li^{+}$ composite: Boosting phosphor stability, optical thermometry, flexible displays and data protection applications. **Materials Today Sustainability**, v. 27, p. 100840, 2024. DOI: 10.1016/j.mtsust.2024.100840. Available in: https://www.sciencedirect.com/science/article/pii/S2589234724001763.

[63] OLIVEIRA, H. H. S.; CEBIM, M. A.; DA SILVA, A. A.; DAVOLOS, M. R. Structural and Spectroscopic Studies of Pr^{3+}-Doped $GdAlO_3$. **IEEE Transactions on Nuclear Science**, v. 57, p. 1260-1263, 2010. DOI: 10.1109/TNS.2009.2036177. Available in: https://ieeexplore.ieee.org/abstract/document/5485135.

[64] WELLER, M.; OVERTON, T.; ROURKE, J.; ARMSTRONG, F. **Química inorgânica**. 6. ed. Porto Alegre: Bookman, 2017. *E-book.* p.835. ISBN 9788582604410. Available in: https://app.minhabiblioteca.com.br/reader/books/9788582604410/.

[65] OLIVEIRA, H. H. S.; CEBIM, M. A.; DA SILVA, A. A.; DAVOLOS, M. R. Structural and optical properties of $GdAlO_3:RE^{3+}$ (RE = Eu or Tb) prepared by the Pechini method for application as X-ray phosphors. **Journal of Alloys and Compounds**, v. 488, p. 619-623, 2009. DOI: 10.1016/j.jallcom.2009.04.099. Available in: https://www.sciencedirect.com/science/article/pii/S092583880900810X.

[66] ELHAMDI, I.; SOUISSI H.; KAMMOUN, S.; DHAHRI, E.; PINA, J.; COSTA, B. F. O.; BRITO, A. L. B.; FAUSTO, R.; LÓPEZ-LAGO E. Structural and luminescent properties of a Cr^{3+}/Sm^{3+} doped $GdAlO_3$ orthorhombic perovskite for solid-state lighting applications. **RSC Advances**, v. 15, p. 2066-2077, 2025. DOI: 10.1039/d4ra09098e. Available in: https://www.sciencedirect.com/org/science/article/pii/S2046206925001810.

[67] TAMRAKAR, R. K.; UPADHYAY, K.; SAHU, M. Spectral characterization of Er^{3+}, Yb^{3+} co doped $GdAlO_3$ phosphor prepared by solid state reaction method. **Journal of Alloys and Compounds**, v. 689, p. 702-712, 2016. DOI: 10.1016/j.jallcom.2016.07.327. Available in: https://www.sciencedirect.com/science/article/pii/S0925838816323623.

[68] KUMAR, P.; SINGH, D.; GUPTA, I.; SINGH, S.; KUMAR, V.; KUMAR, H.; CHHIKARA, S. K. Perovskite $GdAlO_3$:Dy^{3+} nanophosphors: A gel-combustion synthesis, phase evaluation and down conversion luminescent characteristics for lighting applications. **Journal of Luminescence**, v. 252, p. 119409, 2022. DOI: 10.1016/j.jlumin.2022.119409. Available in: https://www.sciencedirect.com/science/article/pii/S0022231322006846.

[69] DENG, T.; YAN, S.; HU, J. Effect of Calcination Temperature on Up-Conversion Photoluminescence of the $GdAlO_3$: Er^{3+},Yb^{3+} Phosphor. **ECS Journal of Solid State Science and Technology**, v. 4, p. R48-R53, 2015. DOI: 10.1149/2.0101503jss. Available in: https://iopscience.iop.org/article/10.1149/2.0101503jss/meta.

[70] DENG, T.; JIANG, X.; ZHANG, Q. Sustainably Adjusting the Up-Conversion White-Emitting Luminescence Properties of $GdAlO_3$: Er^{3+}/Yb^{3+}/Tm^{3+} Phosphors. **Frontiers in Chemistry**, v. 8, p. 788, 2020. DOI: 10.3389/fchem.2020.00788. Available in: https://www.frontiersin.org/journals/chemistry/articles/10.3389/fchem.2020.00788/full.

[71] MAZELSKY, R.; KRAMER, W. E.; HOPKINS, R. H. Crystal growth of $GdAlO_3$. **Journal of Crystal Growth**, v. 2, p. 209-214, 1968. DOI: 10.1016/0022-0248(68)90003-1. Available in: https://www.sciencedirect.com/science/article/pii/0022024868900031.

[72] ROSS, N. L.; ZHAO, J.; ANGEL, R. J. High-pressure structural behavior of $GdAlO_3$ and $GdFeO_3$ perovskites. **Journal of Solid State Chemistry**, v. 177, p. 3768-3775, 2004. DOI: 10.1016/j.jssc.2004.07.002. Available in: https://www.sciencedirect.com/science/article/pii/S0022459604003809.

[73] KONG, L. B.; ZHANG, T. S.; MA, J.; BOEY, F. Progress in synthesis of ferroelectric ceramic materials via high-energy mechanochemical technique. **Progress in Materials Science**, v. 53, p. 207-322, 2008. DOI: 10.1016/j.pmatsci.2007.05.001. Available in: https://www.sciencedirect.com/science/article/pii/S0079642507000266.

[74] TAMRAKAR, R. K.; UPADHYAY, K.; SAHU, M. Spectral characterization of Er^{3+}, Yb^{3+} co doped $GdAlO_3$ phosphor prepared by solid state reaction method. **Journal of Alloys and Compounds**, v. 689, p. 702-712, 2016. DOI: 10.1016/j.jallcom.2016.07.327. Available in: https://www.sciencedirect.com/science/article/pii/S0925838816323623.

[75] KINGSLEY, J. J.; PEDERSON, L. R. Energetic materials in ceramics synthesis. **MRS Proceedings**, v. 296, p. 361-366, 1993. DOI: 10.1557/PROC-296-361. Available in:

https://www.cambridge.org/core/journals/mrs-online-proceedings-library-archive/article/abs/energetic-materials-in-ceramics-synthesis/BFB2428FF0851F707853555E9280EE90.

[76] EKAMBARAM, S.; PATIL, K.C.; MAAZA, M. Synthesis of lamp phosphors: facile combustion approach. **Journal of Alloys and Compounds**, v. 393, p. 81-92, 2005. DOI: 10.1016/j.jallcom.2004.10.015. Available in: https://www.sciencedirect.com/science/article/pii/S0925838804013532.

[77] XU, B.; CAI, J.; HOU, M.; ZHU, MEITING.; SHENG, X.; WANG, H.; PAN, L. Fluorescent structured color pigments based on CB@SiO_2/CQDs core-shell nanospheres for solvent/UV dual-responsive anti-counterfeiting coating, **Dyes and Pigments**, v. 238, p. 112644, 2025. DOI: 10.1016/j.dyepig.2025.112644. Available in: https://www.sciencedirect.com/science/article/pii/S0143720825000142.

[78] STÖBER, W.; FINK, A.; BOHN, E. Controlled growth of monodisperse silica spheres in the micron size range, **Journal of Colloid and Interface Science**, v. 26, p. 62-69, 1968. DOI: 10.1016/0021-9797(68)90272-5. Available in: https://www.sciencedirect.com/science/article/pii/0021979768902725.

[79] MUTTI, A. M. G.; CANISARES, F. S. M.; SANTOS, J. A. O.; SANTOS, B. C.; CAVALCANTE, D. G. S. M.; JOB, A. E.; PIRES, A. M.; LIMA, S. A. M. Silica-based nanohybrids containing europium complexes covalently grafted: structural, luminescent, and cell labeling investigation, **Journal of Sol-Gel Science and Technology**, v. 107, p. 754-770, 2023. DOI: 10.1007/s10971-023-06138-2. Available in: https://link.springer.com/article/10.1007/s10971-023-06138-2.

[80] FERNANDES, R. S.; RAIMUNDO JR, I. M.; PIMENTEL, M. F. Revising the synthesis of Stöber silica nanoparticles: A multivariate assessment study on the effects of reaction parameters on the particle size, **Colloids and Surfaces A**, v. 577, p. 1-7, 2019. DOI: 10.1016/j.colsurfa.2019.05.053. Available in: https://www.sciencedirect.com/science/article/pii/S092777571930473X.

[81] GIRISH, H. N.; BASAVALINGU, B.; SHAO G.-Q.; SAJAN, C. P.; VERMA, S. K. Hydrothermal synthesis and characterization of polycrystalline gadolinium aluminum perovskite ($GdAlO_3$, GAP), **Materials Science-Poland**, v. 33, p. 301-305, 2015. DOI: 10.1515/msp-2015-0045. Available in: https://sciendo-parsed.s3.eu-central-1.amazonaws.com/64724f72215d2f6c89dc3c9e/10.1515.

[82] ALTAMIRANO, D. N.; ANGELES, A. A. B.; RUIZ, J. L.; VALDES, M. A. U.; SOTOLONGO, A. A.; MARQUEZ, J. G. G.; ROMERO, R. A.; MEDINA, J. Z.; MONTALVO, T. R. Thermoluminescent studies of $GdAlO_3$ powders, **Applied Radiation and Isotopes**, v. 186, p. 110268, 2022. DOI: 10.1016/j.apradiso.2022.110268. Available in: https://www.sciencedirect.com/science/article/pii/S0969804322001634.

[83] TAMRAKAR, R. K.; TIWARI, S.; UPADHYAY, K.; ROBINSON, C. S. Synthesis, structural and luminescent properties of Eu^{2+}/Dy^{3+} activated $GdAlO_3$ phosphors by solid state reaction method under nitrogen atmosphere, **Optik**, v. 181, p. 1158-1162, 2019. DOI:

10.1016/j.ijleo.2018.12.076. Available in: https://www.sciencedirect.com/science/article/pii/S003040261832000X.

[84] ZHANG, P.; GAO, M.; GUO, R.; XU, J.; WANG, Y.; LUO, L. Structural and optical properties of $GdAlO_3:Tb^{3+}$ crystal obtained by optical floating zone method, **Optik**, v. 239, p. 166880, 2021. DOI: 10.1016/j.ijleo.2021.166880. Available in: https://www.sciencedirect.com/science/article/pii/S0030402621005829.

[85] CIZAUSKAITE, S.; REICHLOVA, V.; NENARTAVICIENA, G.; BEGANSKIENE, A.; PINKAS, J.; KAREIVA, A. Sol–gel preparation and characterization of gadolinium aluminate, **Materials Chemistry and Physics**, v. 102, p. 105-110, 2007. DOI: 10.1016/j.matchemphys.2006.11.016. Available in: https://www.sciencedirect.com/science/article/pii/S025405840600304X.

[86] KUMAR, P.; SINGH, D.; GUPTA, I.; SINGH, S.; KUMAR, V. Structural and luminescent characteristics of orthorhombic $GdAlO_3:Sm^{3+}$ nanocrystalline materials for solid state lighting, **Chemical Physics Letters**, v. 812, p. 140277, 2023. DOI: 10.1016/j.cplett.2022.140277. Available in: https://www.sciencedirect.com/science/article/pii/S0009261422009344.

[87] KUMAR, P.; SINGH, D.; GUPTA, I.; SINGH, S.; KUMAR, V.; KUMAR, H.; CHHIKARA, S. K. Cool green light emitting $GdAlO_3:Tb^{3+}$ perovskite nanomaterials: Crystal structure and spectroscopic characteristics for advance display appliances, **Inorganic Chemistry Communications**, v. 145, p. 110064, 2022. DOI: 10.1016/j.inoche.2022.110064. Available in: https://www.sciencedirect.com/science/article/pii/S1387700322008723.

[88] TAMRAKAR, R. K.; UPADHYAY, K.; BISEN, D. P. Variation in luminescence behavior of Yb^{3+} doped $GdAlO_3$ phosphor with gradual increase in Yb^{3+} concentration, **Infrared Physics & Technology**, v. 75, p. 160-167, 2016. DOI: 10.1016/j.infrared.2015.12.029. Available in: https://www.sciencedirect.com/science/article/pii/S1350449515300724.

[89] HU, S.; ZHAO, W.; HUANG, X.; YANG, X.; ZHANG, J.; LIN, L.; NI, H.; ZHONG, J. The preparation and luminescence properties of $Gd_2SiO_5:Tb^{3+}@SiO_2$ core-shell spherical particles, **Journal of Alloys and Compounds**, v. 1010, p. 177805, 2025. DOI: 10.1016/j.jallcom.2024.177805. Available in: https://www.sciencedirect.com/science/article/pii/S0925838824043937.

[90] TONG, N. B.; SI, L. V.; DUNG, C. T. M.; HANH, T. T. K.; LAM, T. T. N.; THANG, P. B.; BINH, D. H.; UYEN, N. T. N.; VAN, T. T. T. Intense green upconversion in core-shell structured $NaYF_4$:Er,Yb@SiO_2 microparticles for anti-counterfeiting printing. **Ceramics International**, v. 49, p. 28484-28491, 2023. DOI: 10.1016/j.ceramint.2023.06.105. Available in: https://www.sciencedirect.com/science/article/pii/S0272884223016863.

[91] DWIVEDI, A.; ANURADHA.; SRIVASTAVA, M.; SRIVASTAVA, A.; KUMAR, R.; SRIVASTAVA, S. K. Enhance photoluminescence properties of Ca-Eu:Y_2O_3@SiO_2 core–shell nanomaterial for the advanced forensic and LEDs applications. **Spectrochimica Acta Part A: Molecular and Biomolecular Spectroscopy**, v. 299, p. 122782, 2023. DOI: 10.1016/j.saa.2023.122782. Available in: https://www.sciencedirect.com/science/article/pii/S1386142523004675.

[92] S UAI, P.; GUO, Q.; LIAO, L.; SU, K.; WANG, .; MEI, L.; WOŹN , P.; RUNOWSKI, M. Multi-color $Na_3GaF_6:Tm^{3+},Yb^{3+}@SiO_2$ for dual-mode security and information encryption, **Applied Surface Science**, v. 674, p. 160946, 2024. DOI: 10.1016/j.apsusc.2024.160946. Available in: https://www.sciencedirect.com/science/article/pii/S0169433224016593.

[93] LUO, Y.; GAO, J.; FAN, Z.; YANG, Y.; LING, X.; BAO, J.; LIU, Y.; ZHU, X. Synthesis and luminescent properties of multi-mode core-shell-shell $LaPO_4$:RE (RE^{3+} = Er^{3+}, Eu^{3+}) microspheres for anti-counterfeiting ink applications, **Ceramics International**, v. 51, p. 16817-16827, 2025. DOI: 10.1016/j.ceramint.2024.10.221. Available in: https://www.sciencedirect.com/science/article/pii/S0272884224047412.

[94] MIAO, X.; ZHANG, X.; ZHANG, M.; YU, H.; ZHANG, Y.; SHENG, K.; HAU, J.; XIE, M.; YU, R. Optical properties of the double perovskite $LaGeSbO_6:Eu^{3+}$ phosphor with inversion symmetry under broadband excitation for personal identification and secure anti-counterfeiting ink, **Journal of Alloys and Compounds**, v. 1037, p. 182133, 2025. DOI: 10.1016/j.jallcom.2025.182133. Available in: https://www.sciencedirect.com/science/article/pii/S0925838825036941.

[95] KOSTYUKOV, A. I.; KOSTYUKOVA, N. Y.; NASHIVOCHNIKOV, A. A.; RAKHMANOVA, M. I.; SUPRUN, E. A. Photoluminescent $Y_2O_3:Eu^{3+}$@PVA composite dispersions and films for anti-counterfeiting ink applications, **Optical Materials**, v. 157, p. 116194, 2024. DOI: 10.1016/j.optmat.2024.116194. Available in: https://www.sciencedirect.com/science/article/pii/S0925346724013776.

[96] ZHANG, Y.; CUI, R.; GUO, X.; DING, Z.; DENG, C. A novel thermally-stable red phosphor $CaYGaO_4:Eu^{3+}$ for WLEDs and anti-counterfeiting ink, **Ceramics International**, v. 50, p. 45094-45104, 2024. DOI: 10.1016/j.ceramint.2024.08.349. Available in: https://www.sciencedirect.com/science/article/pii/S0272884224038070.

[97] LI, R.; CUI, R.; CUO, X.; ZHANG, J.; GONG, X.; DENG, C. A novel high-brightness and thermally-stable red phosphor Ca_2GaNbO_6: Eu^{3+} for WLEDs and anti-counterfeiting inks, **Ceramics International**¸ v. 50, p. 50346-50357, 2024. DOI: 10.1016/j.ceramint.2024.09.380. Available in: https://www.sciencedirect.com/science/article/pii/S0272884224044158.

[98] PENG, X.; GUO, X.; CUI, R.; LING-HU, P.; ZHANG, J.; DENG, C. Novel orange red phosphor $BaLaGaO_4$: Sm^{3+} with high quantum efficiency and good thermal stability for indoor illumination and anti-counterfeiting inks applications, **Ceramics International**, v. 50, p. 30111-30123, 2024. DOI: 10.1016/j.ceramint.2024.05.310. Available in: https://www.sciencedirect.com/science/article/pii/S0272884224021898.

[99] ZHANG, Y.; LING, Y.; CUI, R. A novel thermally-stable $Ca_2GaTaO_6:Sm^{3+}$ phosphor and its application in WLEDs and anti-counterfeit inks, **Journal of Rare Earths**, v. 43, p. 1120-1132, 2025. DOI: 10.1016/j.jre.2024.07.001. Available in: https://www.sciencedirect.com/science/article/pii/S00207212400228X.

[100] SHINOHARA, G. M. M. **Influência do agente complexante nas propriedades estruturais e fotoluminescentes do luminóforo vermelho nanoestruturado $Y_2O_3:Eu^{3+}$ via método Pechini**

modificado monitorado por ferramentas de quimiometria. Orientadora: Ana Maria Pires. 2016. Tese (Doutorado em Química) – Instituto de Química, Universidade Estadual Paulista, Araraquara, 2016.

[101] COSTA, A. L.; BISPO-JR, A. G.; LIMA, S. A. M.; PIRES, A. M. Multicolor-emitting luminescent Y_2O_3:RE^{3+}@SiO_2-[RE^{3+}(β-diketone)$_3$] core@shell hybrids featuring dual RE^{3+} activator centers, **Journal of Alloys and Compounds**, v. 843, p. 155811, 2020. DOI: 10.1016/j.jallcom.2020.155811. Available in: https://www.sciencedirect.com/science/article/pii/S0925838820321757.

[102] OLIVEIRA, N. A.; BISPO-JR, A. G.; SHINOHARA, G. M. M.; LIMA, S. A. M.; PIRES, A. M. The influence of the complexing agent on the luminescence of multicolor-emitting Y_2O_3:Eu^{3+},Er^{3+},Yb^{3+} phosphors obtained by the Pechini's method, **Materials Chemistry and Physics**, v. 257, p. 123840, 2021. DOI: 10.1016/j.matchemphys.2020.123840. Available in: https://www.sciencedirect.com/science/article/pii/S0254058420311998.

[103] OLIVEIRA, N. A.; BISPO-JR, A. G.; LIMA, S. A. M.; PIRES, A. M. Red-emitting $BaAl_2O_4$:Eu^{3+} synthesized via Pechini and sol–gel routes: a comparison of luminescence and structure, **Journal of Materials Science**, v. 57, p. 170-184, 2022. DOI: 10.1007/s10853-021-06633-3. Available in: https://link.springer.com/article/10.1007/s10853-021-06633-3.

[104] BISPO-JR, A. G. B.; CECCATO, D. A.; LIMA, S. A. M.; PIRES, A. M. Red phosphor based on Eu^{3+}-isoelectronically doped Ba_2SiO_4 obtained via sol–gel route for solid state lightning, **RSC Advances**, v. 7, p. 53752-53762, 2017. DOI: 10.1039/C7RA10494D. Available in: https://pubs.rsc.org/en/content/articlehtml/2017/ra/c7ra10494d.

[105] BISPO-JR, A. G.; LIMA, S. A. M.; LANFREDI, S.; PRAXEDES, F. R.; PIRES, A. M. Tunable blue-green emission and energy transfer properties in Ba_2SiO_4:Tb^{3+} obtained from sol-gel method, **Journal of Luminescence**, v. 214, p. 116604, 2019. DOI: 10.1016/j.jlumin.2019.116604. Available in: https://www.sciencedirect.com/science/article/pii/S0022231319305101.

[106] BISPO-JR, A. G. B.; LIMA, S. A. M.; CARLOS, L. D.; PIRES, A. M.; FERREIRA, R. A. S. Eu(II)-activated silicates for UV LEDs tuning into warm white light, **Advanced Engineering Materials**, v. 22, p. 20000422, 2020. DOI: 10.1002/adem.202000422. Available in: https://advanced.onlinelibrary.wiley.com/doi/abs/10.1002/adem.202000422.

[107] MESTI, M. E. M. **Luminóforos baseados em $MgAl_2O_4$ do tipo espinélio contendo íons terras raras e metais alcalinos:** Espectroscopia de luminescência de Eu(III) na elucidação da ocupação de sítios. Orientadora: Ana Maria Pires. 2024. Dissertação (Mestrado em Química) – Instituto de Biociências, Letras e Ciências Exatas, Universidade Estadual Paulista, Presidente Prudente, 2024.

[108] GARCIA, A. B. S. **Aluminato de lantânio no planejamento de sistemas *core@shell* luminescentes funcionalizados contendo os íons Eu^{3+} e Tb^{3+} para aplicação em dispositivos conversores de luz**. Orientadora: Ana Maria Pires. 2019. Dissertação (Mestrado em Química) – Instituto de Biociências, Letras e Ciências Exatas, Universidade Estadual Paulista, Presidente Prudente, 2019.

[109] GARCIA, A. B. S. **Desenvolvimento de sistemas ópticos para termometria com aluminato de lantânio dopado com terras raras em estrutura do tipo caroço casca (*core shell*)**. Orientadora: Ana Maria Pires. 2024. Tese (Doutorado em Química) – Instituto de Química, Universidade Estadual Paulista, Araraquara, 2024.

[110] GARCIA, A.B.S.; BISPO-JR, A.G.; LIMA, S.A.M.; PIRES, ANA M. Effects of the Pechini's modified synthetic route on structural and photophysical properties of Eu^{3+} or Tb^{3+}-doped $LaAlO_3$. **Materials Research Bulletin**, v. 143, p. 111462, 2021. DOI: 10.1016/j.materresbull.2021.111462. Available in:https://www.sciencedirect.com/science/article/pii/S002554082100259 2?via%3Dihub.

[111] GARCIA, A.B.S.; M.R. DAVOLOS, MARIAN R.; LIMA, SERGIO A.M.; PIRES, ANA M. Core@shell strategies to enhance green upconversion emission of $LaAlO_3:Er^{III},Yb^{III}$ nanoparticles. **Journal of Luminescence**, v. 272, p. 120653, 2024. DOI: 10.1016/j.jlumin.2024.120653. Available in:https://www.sciencedirect.com/science/article/pii/S0022231324002175.

[112] SARAIVA, L. F.; BISPO-JR, A. G. B.; LIMA, S. A. M.; PIRES, A. M. Eu^{3+}-activated $SrY_2O_4:Ce^{4+/3+}$ red-phosphor for WLEDs: Structural and luminescent insights from experimental and theoretical approaches, **Journal of Alloys and Compounds**, v. 25, p. 168595, 2023. DOI: 10.1016/j.jallcom.2022.168595. Available in: https://www.sciencedirect.com/science/article/pii/S0925838822049866.

[113] LYLE, S. J.; RAHMAN, M. M. Complexometric titration of yttrium and the lanthanons—I: A comparison of direct methods. **Talanta**, v. 10, n. 11, p. 1177–1182, 1963. DOI: 10.1016/0039-9140(63)80170-8. Available in: https://www.sciencedirect.com/science/article/pii/0039914063801708.

[114] PŘIBIL, R. Present state of complexometry—IV: Determination of rare-earths. **Talanta**, v. 14, n. 6, p. 619–627, 1967. DOI: 10.1016/0039-9140(67)80028-6. Available in: https://www.sciencedirect.com/science/article/pii/0039914067800286.

[115] VOGEL, A. I. **Quantitative Chemical Analysis**. 5 ed. Longmans: Green & Co., 1951.

[116] YAPPERT, M.C.; DUPRE, D.B. Complexometric Titrations: Competition of Complexing Agents in the Determination of Water Hardness with EDTA. **Journal of Chemical Education**, v. 74, n. 12, p. 1422-1423, 1997. DOI: 10.1021/ed074p1422. Available in: https://pubs.acs.org/doi/abs/10.1021/ed074p1422.

[117] KUMAR, P.; SINGH, D.; GUPTA, I.; SINGH, S.; KUMAR, V.; KUMAR, H.; CHHIKARA, S.K. Perovskite $GdAlO_3:Dy^{3+}$ nanophosphors: A gel-combustion synthesis, phase evaluation and down conversion luminescent characteristics for lighting applications. **Journal of Luminescence**, v. 252, p. 119409, 2022. DOI: 10.1016/j.jlumin.2022.119409. Available in: https://www.sciencedirect.com/science/article/pii/S0022231322006846.

[118] KUMAR, P.; SINGH, D.; GUPTA, I.; SINGH, S.; KUMAR, V. Emerging green light emission of Er^{3+}-activated single phased $GdAlO_3$ phosphors for lighting applications. **Luminescence**, v. 37,

n. 12, p. 2028-2040, 2022. DOI: 10.1002/bio.4387. Available in: https://analyticalsciencejournals.onlinelibrary.wiley.com/doi/full/10.1002/bio.4387.

[119] KUMAR, P.; SINGH, D.; GUPTA, I.; SINGH, S.; KUMAR, V.; KUMAR, H.; CHHIKARA, S.K. Cool green light emitting $GdAlO_3:Tb^{3+}$ perovskite nanomaterials: Crystal structure and spectroscopic characteristics for advance display appliances. **Inorganic Chemistry Communications**, v. 145, p. 110064, 2022. DOI: 10.1016/j.inoche.2022.110064. Available in: https://www.sciencedirect.com/science/article/pii/S1387700322008723.

[120] TAMRAKAR, R.K.; UPADHYAY, K.; SAHU, M. Spectral characterization of Er^{3+}, Yb^{3+} co doped $GdAlO_3$ phosphor prepared by solid state reaction method, **Journal of Alloys and Compounds**, 689, p. 702-712, 2016. DOI: 10.1016/j.jallcom.2016.07.327. Available in: https://www.sciencedirect.com/science/article/pii/S0925838816323623.

[121] COSTA, A.L.; BISPO-JR, A.G.; LIMA, S.A.M.; PIRES, A.M. Multicolor-emitting luminescent $Y_2O_3:RE^{3+}@SiO_2$-[RE^{3+}(β-diketone)$_3$] core@shell hybrids featuring dual RE^{3+} activator centers. **Journal of Alloys and Compounds**, v. 843, p. 155811, 2020. DOI: 10.1016/j.jallcom.2020.155811. Available in: https://www.sciencedirect.com/science/article/pii/S0925838820321757.

[122] ARMETTA, F.; BOIKO, V.; HRENIAK, D.; PONTERIO R.C.; SALADINO, M.L. Luminescent YPO_4:Eu@PVA dispersions for anti-counterfeiting ink applications. **Materials Letters**, v. 333, p. 133653, 2023. DOI: 10.1016/j.matlet.2022.133653. Available in: https://www.sciencedirect.com/science/article/pii/S0167577X22020080.

[123] XIE, S.; GONG, G.; SONG, Y.; TAN, H.; ZHANG, C.; LI, N.; ZHANG, Y.; XU, L.; XU, J.; ZHENG, J. Design of novel lanthanide-doped core–shell nanocrystals with dual up-conversion and down-conversion luminescence for anti-counterfeiting printing. **Dalton Trans**, v. 48, p. 6971-6983, 2019. DOI: 10.1039/C9DT01298B. Available in: https://pubs.rsc.org/en/content/articlehtml/2019/dt/c9dt01298b.

[124] HOLZWARTH, U.; GIBSON, N. The Scherrer equation versus the 'Debye-Scherrer equation'. **Nature Nanotechnology**, v. 6, p. 534, 2011. DOI: 10.1038/nnano.2011.145. Available in: https://www.nature.com/articles/nnano.2011.145#citeas.

[125] JISHA, P.K., NAIK, R.; PRASHANTHA, S.C.; RAVIKUMAR, C.R.; NAGASWARUPA, H.P.; NAGABHUSHANA, H.; JNANESHWARA, D.M. Synthesis, Diffuse reflectance, Electrical and Photoluminescence properties of nanocrystalline Eu^{3+} doped $GdAlO_3$ Via Combustion method. **Materials Today: Proceedings**, v. 4, p. 11706-11712, 2017. DOI: 10.1016/j.matpr.2017.09.086. Available in: https://www.sciencedirect.com/science/article/pii/S2214785317318199.

[126] SATO, T.; TAKAGI, S.; DELEDDA, S.; HAUBACK, B.C.; ORIMO, S. Extending the applicability of the Goldschmidt tolerance factor to arbitrary ionic compounds. **Scientific Reports**, v. 6, p. 23592, 2016. DOI: doi.org/10.1038/srep23592. Available in: https://www.nature.com/articles/srep23592#citeas.

[127] BARTE, C.J.; SUTTON, C.; GOLDSMITH, B.; OUYANG, R.; MUSGRAVE, C.B.; GHIRINGHELLI, L.M.; SCHEFFLER, M. New tolerance factor to predict the stability of perovskite oxides and halides. **Science Advances**, v. 5, p. 1-9, 2019. DOI: 10.1126/sciadv.aav0693. Available in: https://pmc.ncbi.nlm.nih.gov/articles/PMC6368436/.

[128] SINGH, S.; SIMANTILLEKE, A. P.; SINGH, D. Crystal structure and photoluminescence investigations of $Y_3Al_5O_{12}$:Dy^{3+} nanocrystalline phosphors for WLEDs, **Chemical Physics Letters**, v. 765, p. 138300, 2021. DOI: 10.1016/j.cplett.2020.138300. Available in: https://www.sciencedirect.com/science/article/pii/S0009261420311994.

[129] GLAZER, A.M. The classification of tilted octahedra in perovskites, **Structural Science, Crystal Engineering and Materials**, v. B28, p. 3384-3392, 1972. DOI: doi.org/10.1107/S0567740872007976. Available in: https://journals.iucr.org/paper?buy=yes&cnor=a09401&showscheme=yes&sing=yes.

[130] ZATSEPIN, D. A.; BOUKHVALOV, D. W.; ZATSEPIN, A. F.; KUZNETSOVA, Y. A.; MASHKOVTSEV, M. A.; RYCHKOV, V. N.; SHUR, V. Y.; ESIN, A. A.; KURMAEV, E. Z. Electronic structure, charge transfer, and intrinsic luminescence of gadolinium oxide nanoparticles: Experiment and theory, **Applied Surface Science**, v. 436, 697-707, 2018. DOI: 10.1016/j.apsusc.2017.12.086 0. Available in: https://www.sciencedirect.com/science/article/pii/S0169433217336747.

[131] CHEN, H.; HE, C.; GAO, C.; ZHANG, J.; GAO, S.; LU, H.; NIE, Y.; LI, D.; KAN, S.; ZOU, G. Structural Transition of Gd_2O_3:Eu Induced by High Pressure, **Chinese Physics Letters**, v. 24, 158, 2007. DOI: 10.1088/0256-307X/24/1/043. Available in: https://iopscience.iop.org/article/10.1088/0256- 307X/24/1/043.

[132] QIN, L. S.; WU, Y. T.; SHI, H. S.; CHAI, W. X.; SHU, K. Y.; REN, G. H.; CHEN, X. F. Effects of Doping Lu_2O_3 Into Gd_2O_3 on Phase Transformation and Luminescence, **IEEE Transactions On Nuclear Science**, v. 56, 2979-2982, 2009. DOI: 10.1109/TNS.2009.2026649. Available in: https://ieeexplore.ieee.org/abstract/document/5280504.

[133] VARMA, A.; MUKASYAN, A. S.; ROGACHEV, A. S.; MANUKYAN, V. Solution Combustion Synthesis of Nanoscale Materials, **Chemical Reviews**, v. 116, 14493 – 14586, 2016. DOI: doi.org/10.1021/acs.chemrev.6b00279. Available in: https://pubs.acs.org/doi/10.1021/acs.chemrev.6b00279.

[134] SHYICHUK, A.; JR, R.T.M.; NETO, A.N.C.; RUNOWSKI, M.; ZARAD, M.S.; SZCZESZAK, A.; LIS, S.; MALTA, O.L. Effects of Dopant Addition on Lattice and Luminescence Intensity Parameters of Eu(III)-Doped Lanthanum Orthovanadate, **The Journal of Physical Chemistry C**, v. 120, p. 28497-28508, 2016. DOI: doi.org/10.1021/acs.jpcc.6b10778. Available in: https://pubs.acs.org/doi/full/10.1021/acs.jpcc.6b10778.

[135] TANG, H.; YANG, R.; HUANG, Y. A novel red-emitting Eu^{3+}-doped Na_2MgSiO_4 phosphor with high intensity of $^5D_0 \rightarrow {}^7F_4$ transition, **Journal of Alloys and Compounds**, v. 714, p. 263-269, 2017. DOI: doi.org/10.1016/j.jallcom.2017.04.243. Disponível: https://www.sciencedirect.com/science/article/pii/S0925838817314536.

[136] WU, H.; HAO, Z.; ZHANG, L.; ZHANG, X.; XIAO, Y.; PAN, G.; WU, H.; LUO, Y.; ZHAO, H.; ZHANG, J. Phonon Energy Dependent Energy Transfer Upconversion for the Red Emission in the Er^{3+}/Yb^{3+} System, **The Journal of Physical Chemistry C**, v. 122, p. 9611-9618, 2018. DOI: doi.org/10.1021/acs.jpcc.8b02446. Available in: https://pubs.acs.org/doi/full/10.1021/acs.jpcc.8b02446.

[137] GJHM VAN SARK, W.; DE WILD, J.; RAT, J.K.; MEIJERINK, A.; EL SCHROPP, R. Upconversion in solar cells, **Nanoscale Research Letters**, v. 8, p. 1-10, 2013. DOI: doi.org/10.1186/1556-276X-8-81. Available in: https://link.springer.com/article/10.1186/1556-276X-8-81#citeas.

[138] SHAH, R.; ELDRIDGE, D.; PALOMBO, E.; HARDING, I. Optimisation and Stability Assessment of Solid Lipid Nanoparticles using Particle Size and Zeta Potential, **Journal of Physical Stability**, v. 25, p. 59-75, 2014. Available in: http://web.usm.my/jps/25-1-14/25-1-4.pdf.

[139] DANISH, M.; MUMTAZ, M.W.; FAKHAR, M.; RASHID, U. Response Surface Methodology based Optimized Purification of the Residual Glycerol from Biodiesel Production Process, **Chiang Mai Journal of Science**, v. 44, p. 1570-1582, 2017. Available in: https://www.thaiscience.info/Journals/Article/CMJS/10987601.pdf.

[140] HANRY, E.L.; REDZWAN, N.F.M.; BADEGES, N.F.A.K.; SURUGAU, N. Characterization of biofilms developed from alginate extracted from *Padina sp*. incorporated with calcium chloride ($CaCl_2$), **Journal of Physics: Conference Series**, v. 2314, p. 012022, 2022. DOI: 10.1088/1742-6596/2314/1/012022. Available in: https://iopscience.iop.org/article/10.1088/1742-6596/2314/1/012022/meta.

[141] YAN, Y.; FABER, A.J.; DE WAAL, H. Luminescence quenching by OH groups in highly Er-doped phosphate glasses, **Journal of Non-Crystalline Solids**, v. 181, p. 283-290, 1995. DOI: doi.org/10.1016/S0022-3093(94)00528-1. Available in: https://www.sciencedirect.com/science/article/abs/pii/S0022309394005281.

[142] ABDELRAHMAN, M.S.; KHATTAB, T.A. Recent advances in photoresponsive printing inks for security encoding applications, **Luminescence**, v. 39, p. e4800, 2024. DOI: 10.1002/bio.4800. Available in: https://analyticalsciencejournals.onlinelibrary.wiley.com/doi/full/10.1002/bio.4800.

[143] MESSIER, P.; BAAS, V.; TAFILOWSKI, D.; VARGA, L. Optical Brightening Agents in Photographic Paper, **Journal of the American Institute for Conservation**, v. 44, p. 1-12, 2005. DOI: doi.org/10.1179/019713605806082392. Available in: https://www.tandfonline.com/doi/abs/10.1179/019713605806082392.